Spring 2016

Effect of sparse-build internal structure on performance of fused deposition modeling parts

Shixuan Meng

Department:

EFFECT OF SPARSE-BUILD INTERNAL STRUCTURE ON PERFORMANCE OF FUSED DEPOSITION MODELING PARTS

By
SHIXUAN MENG

A THESIS
Presented to the Faculty of the Graduate School of the
MISSOURI UNIVERSITY OF SCIENCE AND TECHNOLOGY
In Partial Fulfillment of the Requirements for the Degree
MASTER OF SCIENCE IN MECHANICAL ENGINEERING

2016

Approved by

Dr. MING C. LEU
Dr. K. CHANDRASHEKHARA
Dr. HAI-LUNG TSAI

ABSTRACT

Fused deposition modeling (FDM) technology has been used in additive manufacturing for years and is able to significantly reduce both manufacturing time and cost for production tooling and end-use parts. Autoclave molding is one of the conventional tools used to produce composite parts. In autoclave molding, the soft composite material is positioned on the molding tool, and then subjected to vacuum and elevated temperatures to facilitate the curing of the resin. With additive manufacturing (AM), it is possible to fabricate the molding tool with a sparse internal structure, thereby reducing the fabrication time and cost compared to a solid tool. This thesis compares two different approaches to design the sparse internal structure of a mold – by using a sparse double dense structure and by using topology optimization geometry. To ensure a fair comparison, the amount of material used to build the tool is kept constant. Two CAD models are designed, each having three possible internal structure structures: solid, sparse double dense structure, and topology optimization geometry. The physical part of the first CAD model is fabricated and used in a compression experiment to validate the results of finite element analysis (FEA) for the three structures. The second CAD model is an autoclave molding tool. Computer simulation is used to predict the performance of this molding tool with each of the three structures after the accuracy of the FEA solver has been proven with the first model.

ACKNOWLEDGMENTS

There were many people who helped me throughout the last two years. I express my deepest gratitude to my advisor, Dr. Ming C. Leu. My research would have been impossible without his support, advice, and guidance. I thank Dr. K. Chandrashekhara for his constant help, patience, and advice in this research project. I also thank Dr. Hai-lung Tsai for spending his time and effort as one of my committee members and helping me through the course of my studies.

I thank Dr. Balakrishnan's supervision on my teaching assistant position. I thank Ms. Katherine Wagner's great help during graduate school. I thank Leah Mason, Wenjin Tao, Xin Wang, Krishna Prasanth, and Gregory Taylor for their help during this research study. I thank all of my research mates in the VRAM laboratory for their help during my graduate study.

Finally, I deeply appreciate my parents Geping Xie, Wei Meng, parents in law Min Zhao, Feng Guo, my wife Xinyao Guo, and family for their support and encouragement and all my friends who supported me during my studies at Missouri University of Science and Technology.

TABLE OF CONTENTS

Page

ABSTRACT iii

ACKNOWLEDGMENTS iv

LIST OF ILLUSTRATIONS vii

LIST OF TABLES ix

SECTION

1. INTRODUCTION 1
    1.1. BACKGROUND 1
    1.2. OBJECTIVES AND EQUIPMENT 4
2. PARTIAL-PRESSURE MODEL DESIGN AND FINITE ELEMENT ANALYSIS VALIDATION 7
    2.1. SPARSE DOUBLE DENSE DESIGN 7
    2.2. TOPOLOGY OPTIMIZATION APPROACH 8
        2.2.1. Partial-Pressure Model Topology Optimization 8
        2.2.2. Smoothing and Generation of the Partial-Pressure Model 10
    2.3. FINITE ELEMENT ANALYSIS OF PARTIAL-PRESSURE MODEL 13
    2.4. EXPERIMENTAL VALIDATION 17
3. FULL-PRESSURE MODEL OPTIMIZATION 26
    3.1. TOPOLOGY OPTIMIZATION OF THE FULL-PRESSURE MODEL 26
    3.2. SMOOTHING AND GENERATION OF THE FULL-PRESSURE MODEL 27
    3.3. FEA VALIDATION 28
4. OVERALL COMPARISON OF THE THREE DIFFERENT STRUCTURES 33
5. CONCLUSION 37

APPENDICES

A. EXPERIMENT DATA OF COMPRESSION TEST WITH DIFFERENT BUILDING PARAMETERS 38
B. VALIDATION TESTING TOOLS MAXIMUM DISPLACEMENTS 41

C. COORDINATE MEASUREMENT MACHINE DATA 44
D. FINITE ELEMENT ANALYSIS CONVERGENCE STUDY 46
E. BAR CHART DATA 48
BIBLIOGRAPHY 50
VITA 51

LIST OF ILLUSTRATIONS

Page

Figure 1.1 Layer-by-layer fabrication of a part 2
Figure 1.2 Illustration of topology optimization 3
Figure 1.3 Illustration of autoclave composite molding process 3
Figure 1.4 Illustration of Stratasys Fortus 400mc 4
Figure 1.5 Illustration of INSTRON 5985 5
Figure 1.6 Illustration of Brown & Sharpe RefleX 454 6
Figure 2.1 (a) Illustration of sparse double dense cross section; (b) illustration of sparse double dense parameters 7
Figure 2.2 Steps to finalize a topology optimization based optimization 9
Figure 2.3 Illustration of partial-pressure validation testing tool dimensions (mm) 10
Figure 2.4 Illustration of raw topology optimized model 11
Figure 2.5 Cross section view of smoothed partial-pressure model 11
Figure 2.6 (a) Illustration of raw topology optimization internal structure surface fabrication toolpath at different layers; (b) redesigned internal structure surface fabrication toolpath at different layers 12
Figure 2.7 (a) Raw topology optimization internal structure; (b) redesigned internal structure surface fabrication simulation result 14
Figure 2.8 (a) Compression test set up; (b) FEA compression test model 14
Figure 2.9 (a) Cross section view of sparse double dense pattern; (b) illustration of linear pattern for thin wall and shell element thin wall composition 15
Figure 2.10 Maximum displacements of three partial-pressure models 16
Figure 2.11 Stratasys Fortus 400mc 17
Figure 2.12 (a) INSTRON 5985 compression testing machine; (b) the load heads 18
Figure 2.13 Pressure vs. displacement for the solid model 19
Figure 2.14 Pressure vs. displacement for the sparse double dense model 19
Figure 2.15 Pressure vs. displacement for the topology optimized model 20
Figure 2.16 Illustration of average linearized result compared to nonlinear results 20
Figure 2.17 Linearized Pressure-displacement relationships 21
Figure 2.18 Displacement comparison between FEA and experiment with solid, sparse double dense, and topology optimized design 22

Figure 2.19 (a) Brown & Sharpe RefleX 454 CMM; (b) illustration of dimensions measurements 23

Figure 2.20 Illustration of fixture calibration 24

Figure 3.1 A pressure of 0.6895 MPa (100 psi) pressure evenly distributed on the top and side surfaces in topology optimization 26

Figure 3.2 Illustration of topology optimization results with different mesh densities; black oval shows the location of maximum deformation 27

Figure 3.3 Illustration of redesigned topology optimization models with different numbers of stiffeners 28

Figure 3.4 Maximum von Mises stresses with different number of stiffeners 29

Figure 3.5 Maximum displacements with different number of stiffeners 29

Figure 3.6 Illustration of von Mises stress with ten stiffeners 30

Figure 3.7 Illustrations of displacement in z-direction 30

Figure 3.8 Illustrations of resultant displacement among the three different designs 31

Figure 3.9 Illustrations of dimples in sparse double dense full-pressure FEA 32

Figure 4.1 Overall FEA, fabrication performance comparison of the partial-pressure model 34

Figure 4.2 Overall FEA, fabrication performance comparison of the full-pressure model 35

LIST OF TABLES

Page

Table 2.1 ULTEM 9085 material properties at room temperature [11] 15
Table 2.2 Partial-pressure model fabrication and FEA simulation results 16
Table 2.3 Partial-pressure model dimensions before compression test 25
Table 2.4 Partial-pressure model dimensions after compression test 25
Table 3.1 Fabrication and FEA simulation results of three full-pressure models 32

1. INTRODUCTION

1.1. BACKGROUND

Shortening the product development cycle time is a key factor in ensuring that a company remains ahead of its competitors. Additive manufacturing (AM) is a method of rapidly fabricating a physical part based on a design model. It has been used in various industries over the past three decades [1]. It is an efficient tool to help designers quickly implement their designs into reality. One of the major advantages of AM is that the build time for product development is shortened significantly. Furthermore, AM enables light-weight parts to be manufactured by changing the internal structure of the model from solid to sparse. The use of AM to fabricate the molding tool subverts the traditional concept of a molding tool, as it takes considerably less time to produce high-quality molding tools [2].

Fused deposition modeling (FDM) is an AM method that builds parts of nearly any geometry by accumulating the extrusion of many two-dimensional layers, as shown in Figure 1.1. Thermoplastic filaments are heated up by a liquefier and then extruded through the tip of a nozzle. The FDM approach enables the production of complex structures. There are numerous approaches to build design models. One effective approach of sparse-build FDM is to build the inside of the model with a double dense internal structure [3]. In this thesis, the sparse double dense internal structure and an internal geometry obtained by topology optimization are used to investigate building parts with reduced weight or increased stiffness. The topology optimization is implemented with a modification of the model that is tailored for additive manufacturing [4].

Topology optimization (TO) has become an important research area in structural optimization. It is a mathematical approach that optimizes material distribution within a desired design space after defining a set of loading and boundary conditions [5]. The results of TO can be normally constrained in three ways, i.e., by maximum deformation/displacement, von Mises stress, or material volume. An example is shown in Figure 1.2. The topology optimization software used in this study is Altair SolidThinking

INSPIRE (Altair, Troy, MI), which uses finite element analysis (FEA) to determine the loading of each node in the mesh and removes material based on a set of criteria/constraints. This approach enables the creation of material-efficient structures quickly. Topology optimization may work with a CAD system to help design structural parts, thereby helping to reduce the manufacturing cost, development time, and/or material usage.

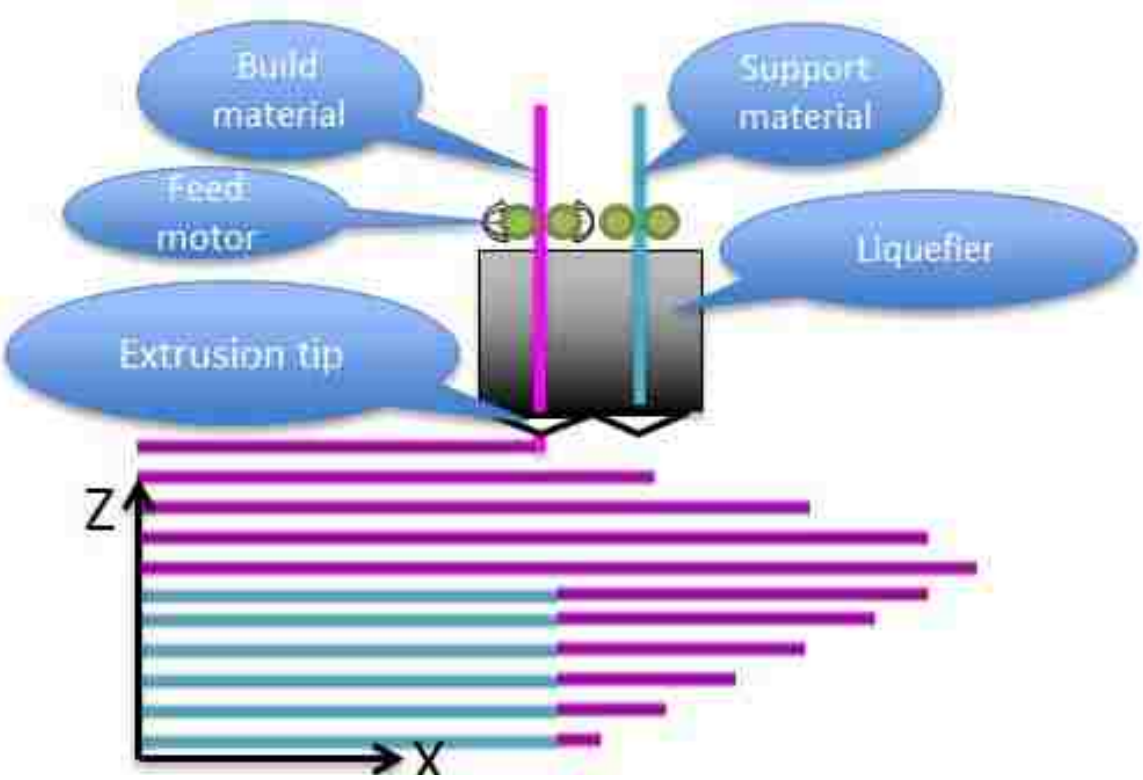

Figure 1.1 Layer-by-layer fabrication of a part

Fused deposition modeling based 3D printers are widely used in modeling, prototyping, and production applications. Increased numbers of possible applications have been continuously discovered using this process. In this thesis, the design and manufacture of an autoclave molding tool is investigated. An autoclave is useful for manufacturing composite parts via pressurization at elevated temperatures. Inside the

chamber, the environment temperature and pressure are increased up to, e.g., 177°C (350°F) and 0.6895 MPa (100 psi). After thermal cycles, the composite part is cured. An illustration of this process is shown in Figure 1.3. The deformation and thermal expansion of the mold significantly affect the dimensional accuracy of the finished composite parts [6].

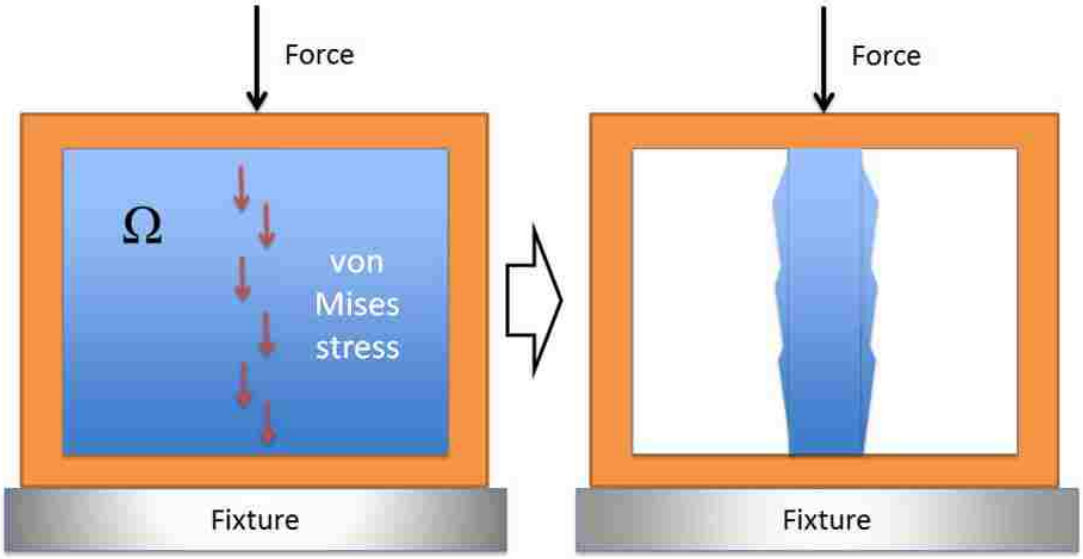

Figure 1.2 Illustration of topology optimization

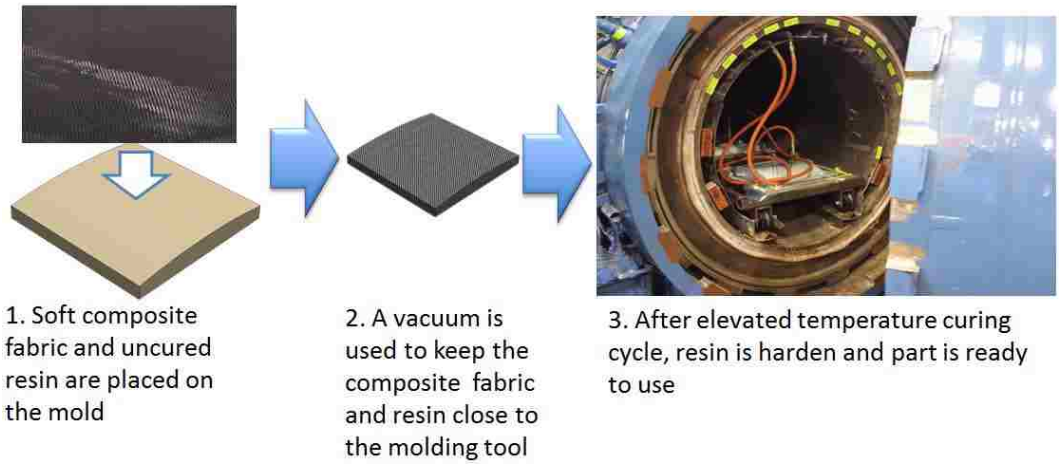

Figure 1.3 Illustration of autoclave composite molding process

1.2. OBJECTIVES AND EQUIPMENT

The objectives of this research are to compare FEA and experiment results to validate the accuracy of the SolidWorks FEA solver, and to predict and compare the performances of different internal structures in an FDM based autoclave molding tool application. In this thesis, three different internal structures (solid, sparse double dense, and topology optimized) are implemented for performance comparison, while keeping the same amount of tool material. Solid internal structure is used as a baseline reference in the comparison.

The FDM machine being used is a Stratasys Fortus 400mc (Stratasys, Eden Prairie, MN) shown in Figure 1.4. The molding tools for testing are fabricated with ULTEM 9085 material and a T16 extrusion tip. The accuracy of Fortus 400mc is ±0.127 mm, thus a tolerance of less than 0.5% in the fabricated part is expected [7].

Figure 1.4 Illustration of Stratasys Fortus 400mc

Since an autoclave was not accessible during this study, FEA was used to simulate autoclave testing results. To ensure the accuracy of the FEA solver, FEA is run on the CAD model of a physical part and the FEA predictions are validated by a compression experiment. The machine used for the compression testing is an INSTRON 5985 (INSTRON, Canton, MA) shown in Figure 1.5. Since this machine is not capable of producing the same pressure conditions as an autoclave, a FEA model for partial-pressure compression test is developed by modifying the autoclave full-pressure FEA model. This partial-pressure model has a flat top to accommodate the INSTRON machine, which produces a uniform pressure on the top of the physical model. A load vs. displacement chart is plotted after recording the compression test data [8].

Figure 1.5 Illustration of INSTRON 5985

To ensure that the dimensions of the parts fabrication are within an adequate tolerance and to determine if plastic deformation has occurred, a coordinate measurement machine (CMM) is used to measure the modified molding tool before and after the compression experiment. The CMM is a Brown & Sharpe RefleX 454 (Brown & Sharpe, North Kinstown, RI) shown in Figure 1.6, which uses a probe to measure the positions of various points on the molding tool. Precise dimensions are calculated after the coordinate locations have been collected from the testing tools.

Figure 1.6 Illustration of Brown & Sharpe RefleX 454

The topology optimization models are created using the Altair SolidThinking INSPIRE (Altair, Troy, MI) software. The FEA simulations are conducted using the SolidWorks (Dassault Systemes, Vélizy-Villacoublay, France) FEA solver. After a CAD molding tool has been designed, Stratasys Insight is used to generate the fabrication toolpath and upload the toolpath to the Stratasys Fortus 400mc.

2. PARTIAL-PRESSURE MODEL DESIGN AND FINITE ELEMENT ANALYSIS VALIDATION

2.1. SPARSE DOUBLE DENSE DESIGN

The sparse build part has the intent of minimizing building material and build time. However, the existing knowledge of using FDM rapid tooling and manufacturing and the performance data of the sparse double dense build parts are very limited. In this thesis, the maximum von Mises stress, maximum displacement, and other molding tool fabrication performance factors are investigated and compared with different internal structures. The sparse double dense parameters used in this study are shown in Figure 2.1.

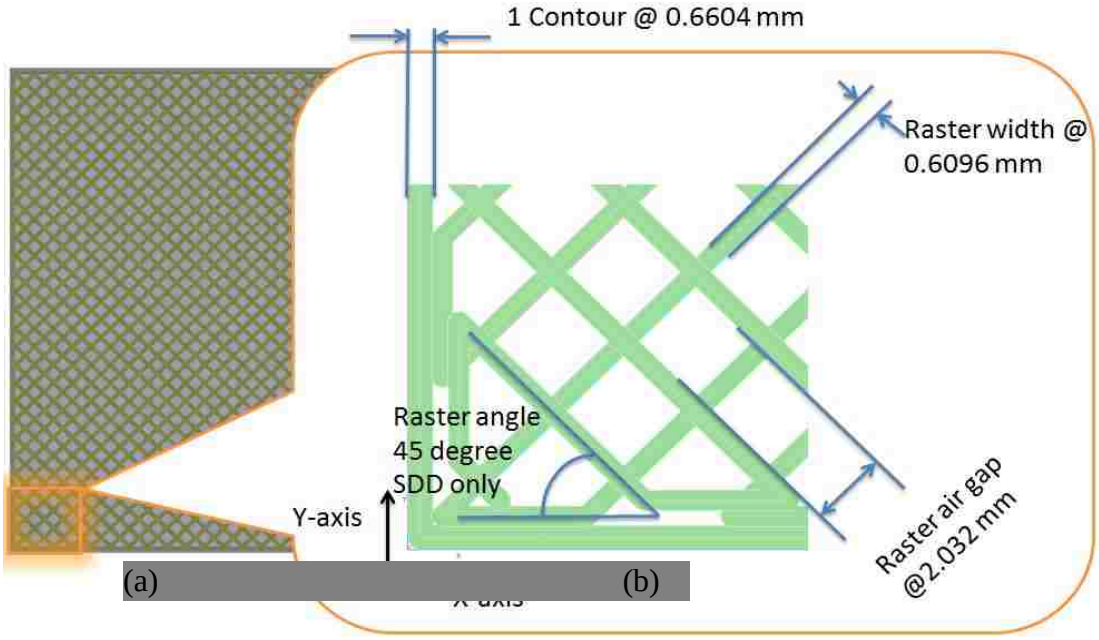

Figure 2.1 (a) Illustration of sparse double dense cross section; (b) illustration of sparse double dense parameters

The sparse double dense structure is a light-weight internal structure commonly used in FDM tooling and manufacturing applications. This internal structure has the

advantages of reduced amount of build material, shorter build time, and higher strength to mass ratio compared to a solid structure. The raster air gap is chosen based on a previous study of Dr. Ming C. Leu and his associates [2], which shows the relationship between decreasing the air gap size and increasing the compressive modulus. The experiment data of compression test with different building parameters from that study can be found in Appendix A. A single contour, or layer outline, is chosen since the focus of this study is on the effect of internal structure. Since the extrusion tip, T16, is capable of extrusion width from 0.4 mm to 0.8 mm, a width slightly larger than the midpoint of 0.6 mm is chosen.

2.2. TOPOLOGY OPTIMIZATION APPROACH

A simplified validation of the autoclave molding tool is conducted to prove the SolidWorks FEA solver's accuracy of predicting stiffness and deformation in our study. Hence the load is only applied on about one third of the top surface, which is flattened, and a compression experiment is performed to validate the FEA predictions. After the solver's accuracy has been verified, an autoclave FEA model is conducted to predict the performance of each internal structure at room temperature.

2.2.1. Partial-Pressure Model Topology Optimization. A topology optimization can be performed based on volume, stress or displacement constraint. In this thesis, the volume constraint is used such that a fair comparison can be made between the two internal structures. The format of mold geometry with the best compatibility is the STEP file because based on the experience indicates that the STL file does not work properly with Altair SolidThinking INSPIRE, although the software has the option to import an STL file. The software can export IGES, STEP, PARASOLID or STL files that have adequate mesh density. Topology optimization has mesh dependency, which means the different mesh size will affect the prediction results. Due to the mesh size dependency, the more refined the mesh is, the more accurate the topology optimization results will be. The steps to redesign based on topology optimization is shown in Figure 2.2 and are given in the following:

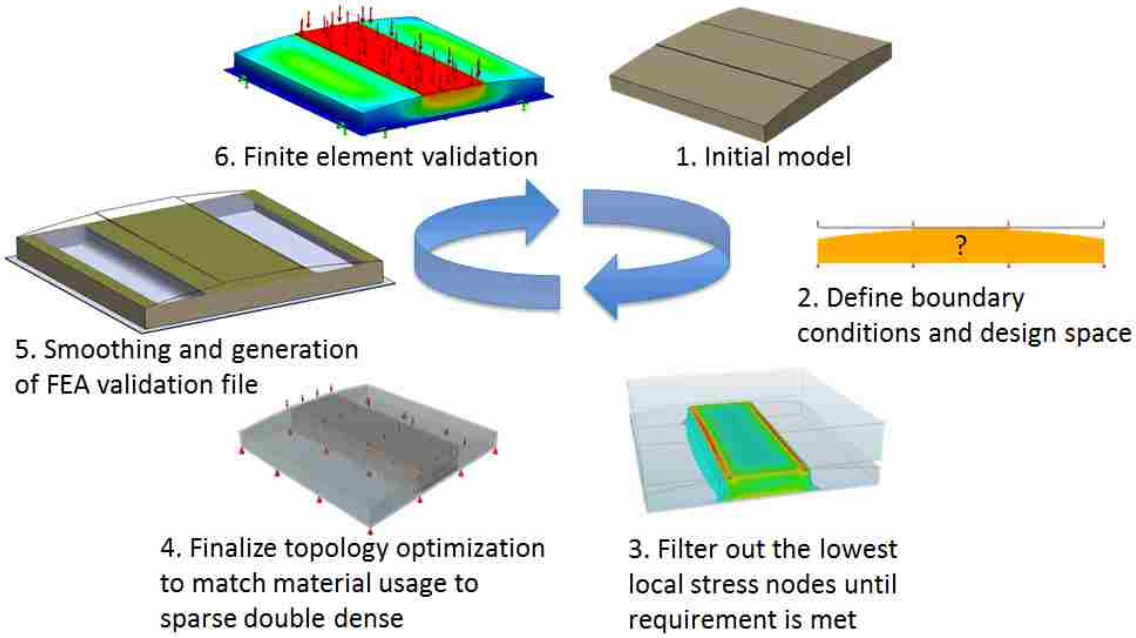

Figure 2.2 Steps to finalize a topology optimization based optimization

1. Design a solid model.

2. Define boundary conditions, design space, and material properties in FEA software.

3. INSPIRE runs an FEA study and uses the obtained numerical data to filter out the nodes that have the smallest von Mises stresses during the iterations until a desired objective is met. In this case the constraint is material volume in order to ensure a fair comparison, thus the amount of material used to build the part is kept constant.

4. After topology optimization iterations, the constraint on material volume is met, a finalized model is outputted.

5. Based on the raw topology optimization, and a smoothed redesign is generated.

6. Use an FEA software to conduct simulations and generate predictions.

The first model, shown in Figure 2.3, is a modified autoclave model to verify the effectiveness of the FEA solver, SolidWorks simulation. A flat top is added to the molding tool. The purpose of the flat top modification is to have an accurate compression

experiment result with INSTRON 5985, which has a flat load head on the top. This model is called the partial-pressure model of the molding tool.

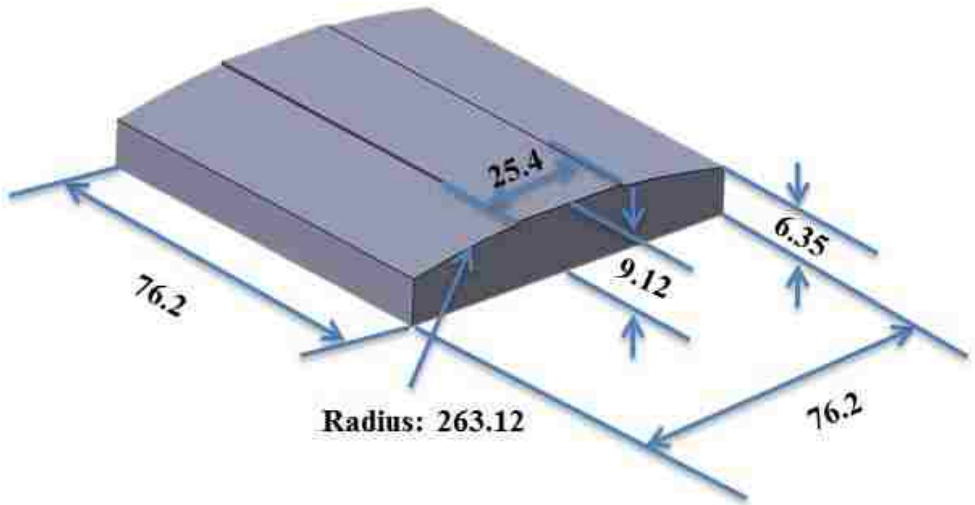

Figure 2.3 Illustration of partial-pressure validation testing tool dimensions (mm)

2.2.2. Smoothing and Generation of the Partial-Pressure Model. Since the sparse double dense design consumes 31.79 cm^3 of build material, the volume of topology optimization model is also the same. After the topology optimization is run as shown in Figure 2.4, it is desirable to redesign the model since the resulted geometry from topology optimization usually has inadequate smoothness, which may lead to low manufacturability and high stress concentration.

To fabricate the physical part from the raw topology optimization model, the build time is estimated to be 92 minutes by Stratasys Insight 10.2, which is expected to reduce with smoothed redesign. Since stress concentration is expected to be improved, smaller deformation and higher safety factor are also expected. The molding tool model is redesigned with smoothed surfaces and rounded edges to improve the performance in terms of von Mises stress, displacement, and build time, while keeping the mass (material volume) unchanged. The redesigned model is shown in Figure 2.5, Compared with the raw topology optimized model, only the width is adjusted to meet the constraint on the

same amount of build material as the model with a sparse double dense internal structure, since the length and height of the stiffener structure in the center are fixed in the molding tool.

The redesigned tool model has two smoothed side faces on the stiffener structure and a much smaller number of edges, therefore the build time estimation of the redesigned model after topology optimization is reduced from 78 minutes to 73 minutes. Figure 2.6 contrasts the extrusion paths between the two models and predicts the fabrication time differences between the two models. The raw topology optimized model has a substantially longer path to traverse the boundary curve than the redesigned model whose boundary consists of only straight edges.

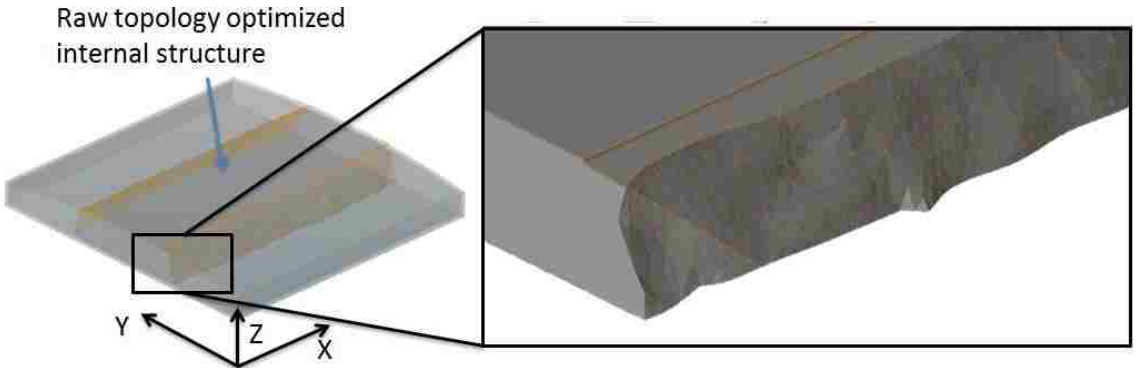

Figure 2.4 Illustration of raw topology optimized model

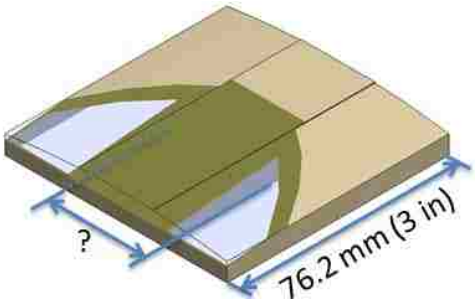

Figure 2.5 Cross section view of smoothed partial-pressure model

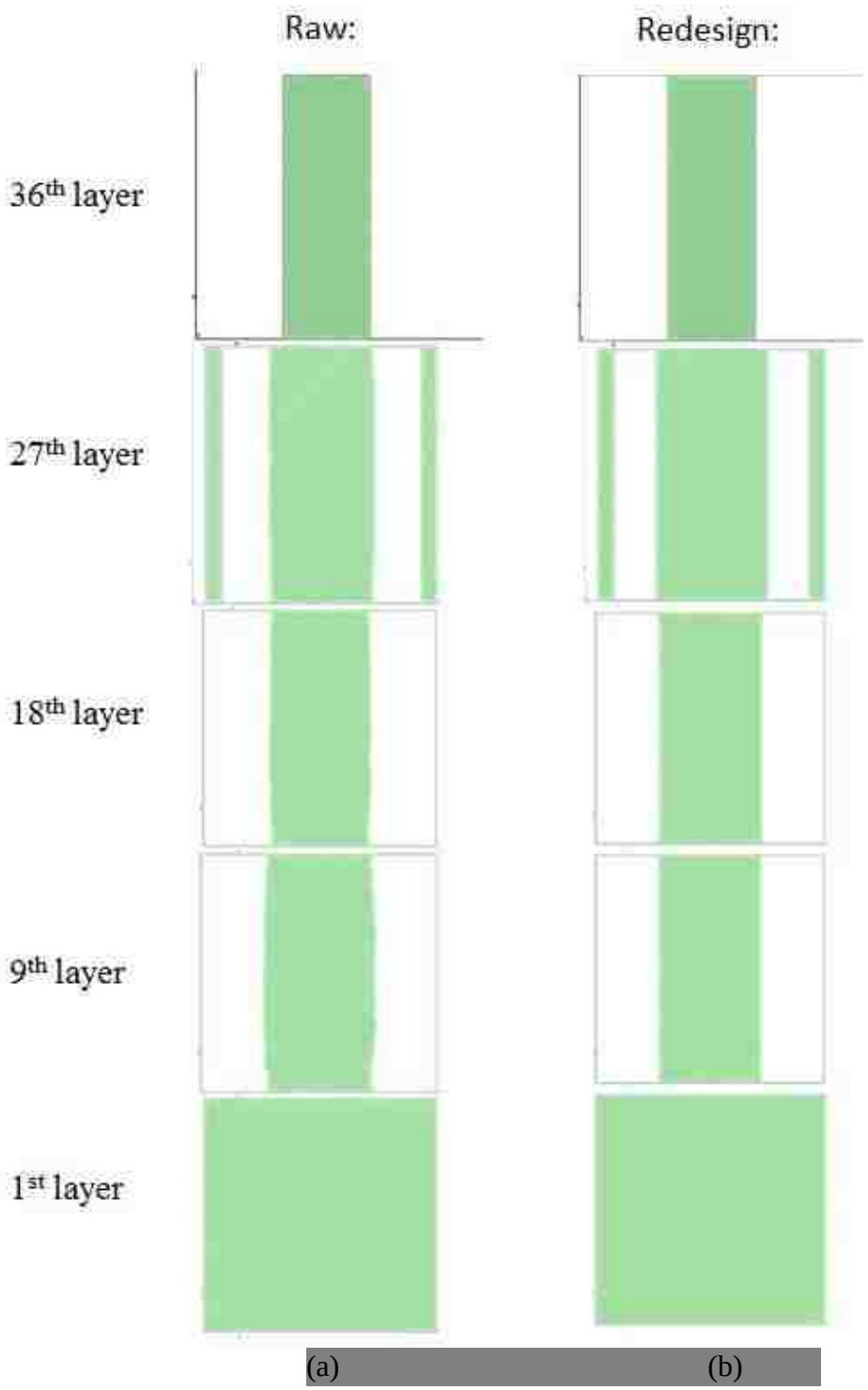

Figure 2.6 (a) Illustration of raw topology optimization internal structure surface fabrication toolpath at different layers; (b) redesigned internal structure surface fabrication toolpath at different layers

2.3. FINITE ELEMENT ANALYSIS OF PARTIAL-PRESSURE MODEL

An FEA study is used to compare the model performance before and after the redesign. Because the results generated by topology optimization shown in Figure 2.4 are coarse and not optimized for manufacturing, redesigns are done in SolidWorks from the topology optimization generated models. Figure 2.6 shows comparisons of the cross-sectional views of the topology optimization model and the refined model. The first figure is the raw topology optimization model, and the second figure is the redesigned model. The FEA result shows that the von Mises stress is reduced from 18.48 MPa to 18.06 MPa. Figure 2.7 shows the geometric details of the cross section for the internal structure of the raw topology optimization model compared to that of the redesigned model.

During the compression test with INSTRON 5985, a load head is placed on top of the part to provide a pressure to the testing part. The bottom load head is fixed. The load condition in the FEA is designed to be the same as the compression experiment, as shown in Figure 2.8, where the two rigid planes are applied as the load heads. The bottom plane is fixed, and the top plane has one degree of freedom in the vertical direction. The contact setting is no penetration, i.e., the testing part does not allow the testing tool to move into the load heads. In other words, the bottom of the model will not deform in the vertical direction.

The shell element is illustrated in Figure 2.9. This technique is used to reduce the computation load including CPU usage and memory requirement when the wall is meshed as shell elements instead of tetrahedral elements. The computer has difficulty in meshing of thin walls with tetrahedral elements due to the much larger number of mesh nodes required. The FEA study uses the SolidWorks linear static simulation solver. The material properties of ULTEM 9085 at room temperature are shown in Table 2.1 [10] [11], which are used as an input in the FEA study.

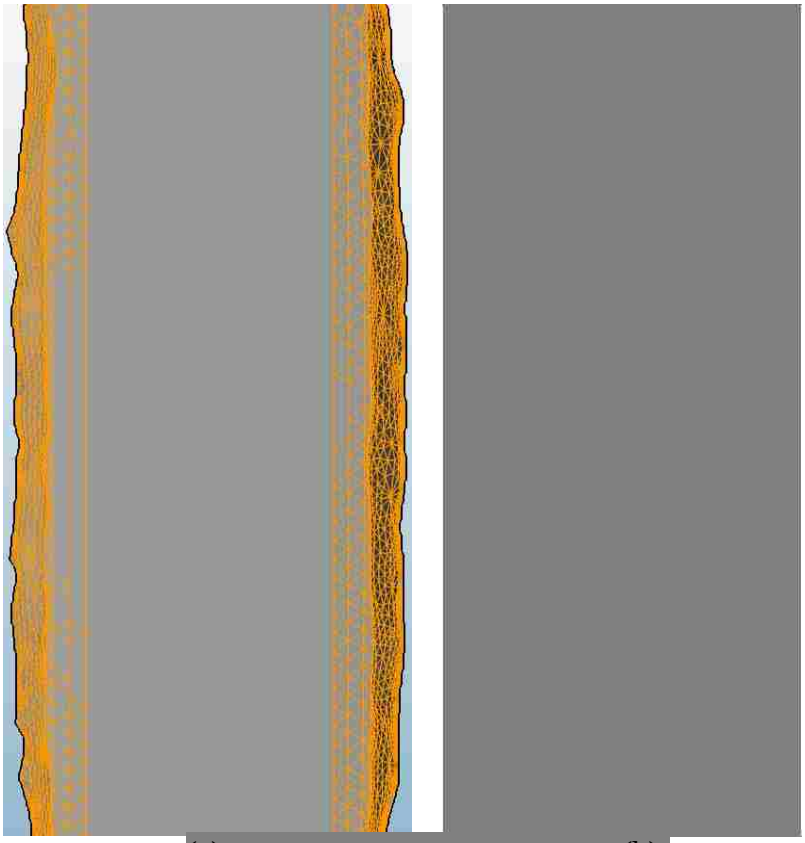

Figure 2.7 (a) Raw topology optimization internal structure; (b) redesigned internal structure surface fabrication simulation result

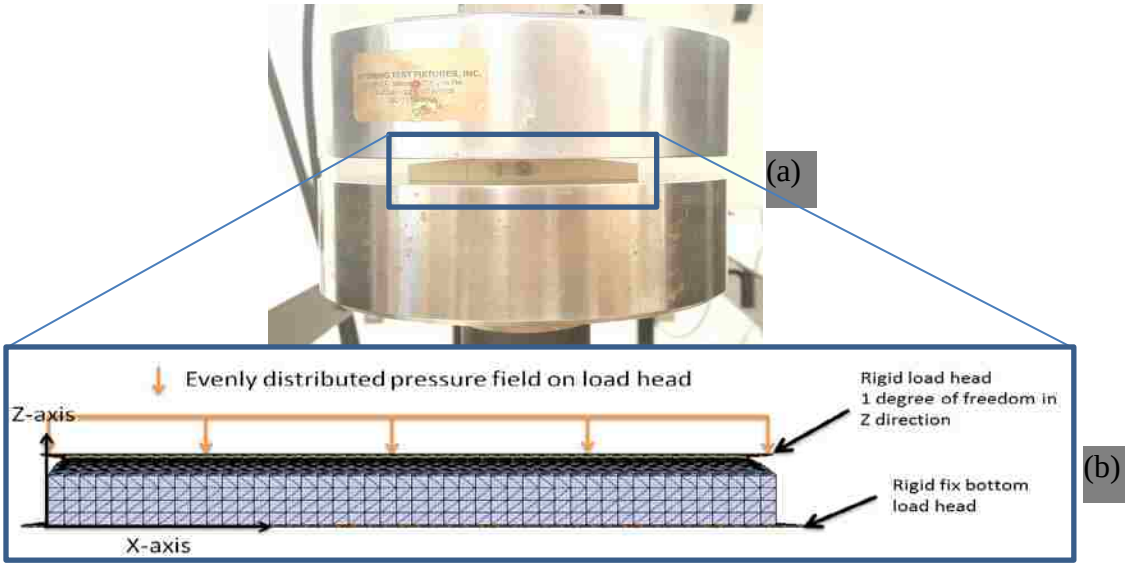

Figure 2.8 (a) Compression test set up; (b) FEA compression test model

Table 2.1 ULTEM 9085 material properties at room temperature [11]

Elastic Modulus (N/m^2)	Poisson's Ratio	Weight Density (N/m^3)	Yield Strength (N/m^2)
$83.8*10^6$	0.4	1211	$49.96*10^6$

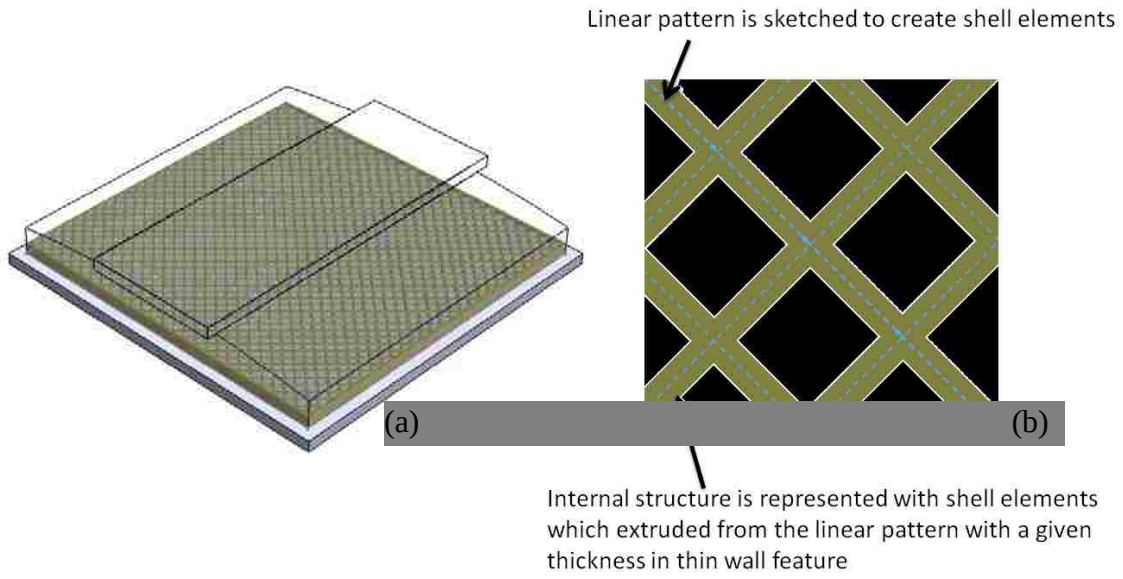

Figure 2.9 (a) Cross section view of sparse double dense pattern; (b) illustration of linear pattern for thin wall and shell element thin wall composition

The FEA predictions of displacements for the three partial-pressure models are shown in Figure 2.10. Since the rigid load head is applying uniformly distributed pressure on the flat top surface, the maximum displacement appears on the entire flat top surface. Therefore, the maximum displacement of the flat top surface can be used to compare to the compression experiment displacement to verify the effectiveness of the FEA solver.

Other performance indexes in terms of the maximum von Mises Stress, material usage, and build time are compared. Fabrication-related performance indexes including material usage and fabrication time are generated by Stratasys Insight software. A detailed comparison is given in Table 2.2. The build time is simulated with Stratasys Control Center. The topology optimization model takes even longer time than the solid

model because it requires a support material besides the part material, and the build head needs to keep changing between the nozzle for the part material and the nozzle for the support material.

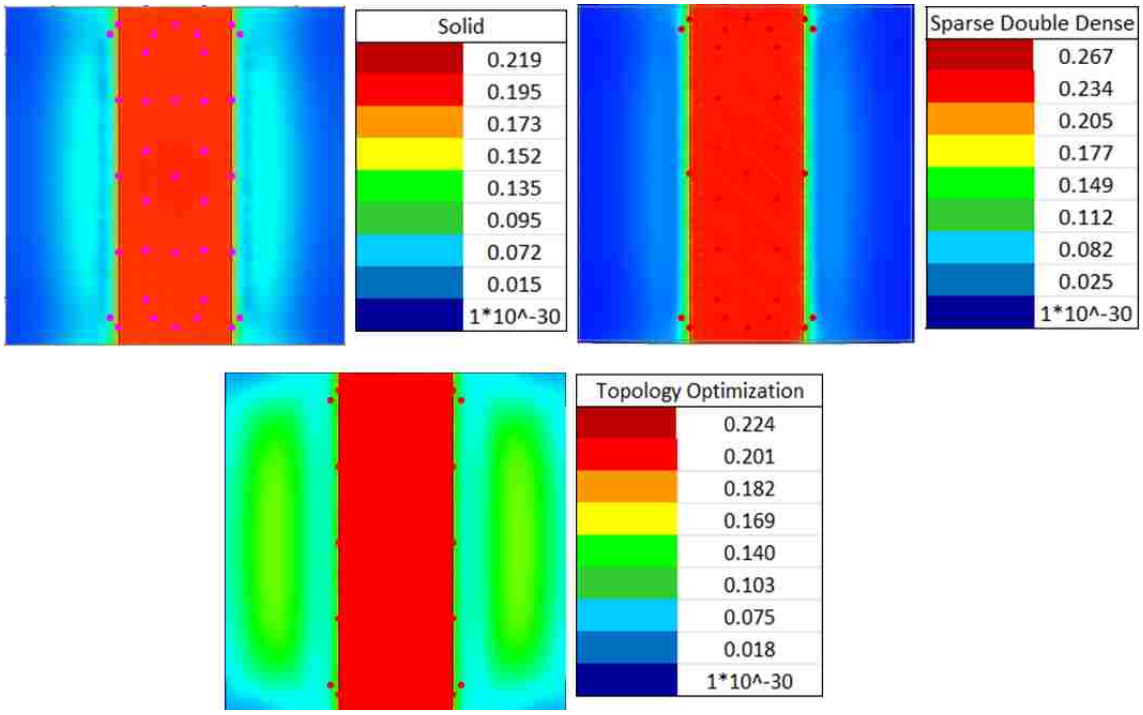

Figure 2.10 Maximum displacements of three partial-pressure models

Table 2.2 Partial-pressure model fabrication and FEA simulation results

	Build Material (cm^3)	Support Material (cm^3)	Build Time (min)	Maximum Displacement (mm)	Maximum von Mises Stress (MPa)
Solid	48.51	1.64	49	0.219	14.65
Sparse Double Dense	31.79	1.64	37	0.267	59.14
Topology Optimization	31.79	7.70	75	0.224	18.06

After completing the FEA for partial-pressure molding tool, a compression test is performed with INSTRON 5985 on the fabricated physical model to validate the FEA predictions. A Stratasys Fortus 400mc is used to fabricate the physical parts with ULTEM 9085 for the molding tool. The Insight software is used to communicate with the Fortus 400mc to upload the toolpath. It also provides estimations on the material amount and build time.

2.4. EXPERIMENTAL VALIDATION

The purpose of the experiment validation is to verify the FEA solver accuracy. A Stratasys Fortus 400mc Fused Deposition Machine, as shown in Figure 2.11, has a heated chamber that reduces the temperature difference between the finished extrusion and a new extrusion so that heat shrinkage is minimized and part accuracy is maximized. The material used to fabricate the model is ULTEM 9085. The partial-pressure model dimensions are shown in Figure 2.3. Two nozzle tips are used to extrude part material and support material. When both materials are used in building each layer, the time of fabrication is expected to increase since the liquefier temperature needs to be adjusted every time when it switches between the materials.

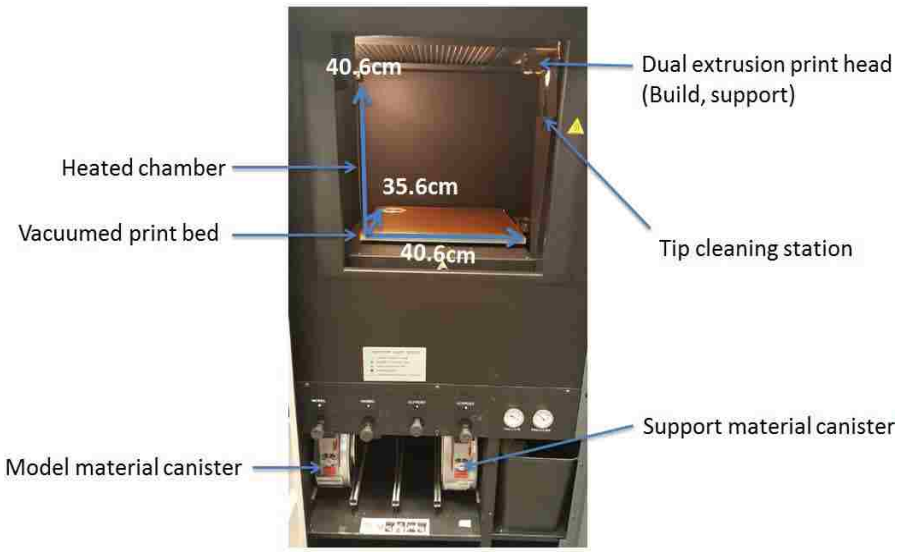

Figure 2.11 Stratasys Fortus 400mc

The build parameters used for the molding tool fabrication are as follows:

- Raster width = 0.6096 mm (0.024”)
- Contour width = 0.6604 mm (0.026”)
- Air gap = 2.032 mm (0.08”) for sparse double dense
- Raster angle = 45^{o}, -45^{o}
- Cap thickness = 0.762 mm (0.03”)

An INSTRON 5985 compression testing machine, as shown in Figure 2.12, is used for the compression test. The top load head provides the load and the bottom load head is fixed. An average load vs. displacement chart is generated for each of the three models: solid model, sparse double dense model, and redesigned topology optimization model. Each model has five test specimens.

Figure 2.12 (a) INSTRON 5985 compression testing machine; (b) the load heads

After all the data are collected from the compression specimens, an average load vs. displacement chart is generated for each model shown in Figures 2.13-2.15, which

show that the solid model starts its linear elastic deformation near 12 MPa, and the sparse double dense and topology optimized models start their linear elastic deformations near 15 MPa.

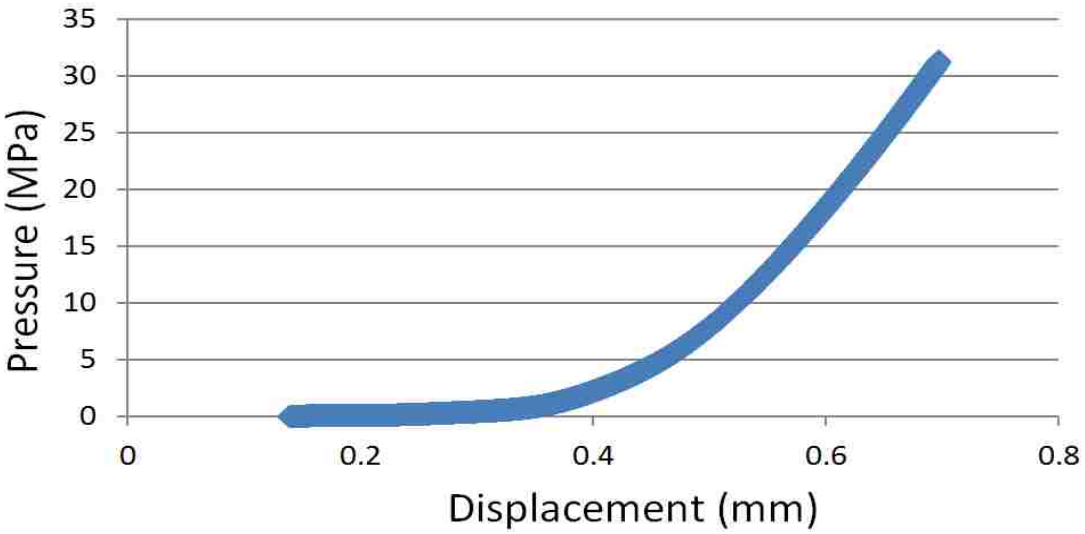

Figure 2.13 Pressure vs. displacement for the solid model

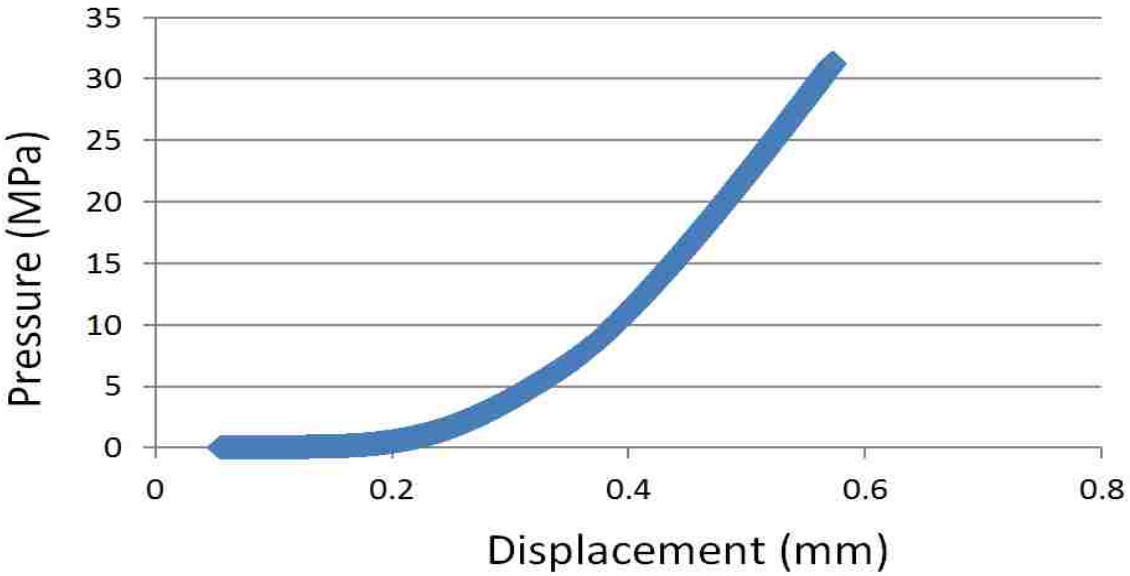

Figure 2.14 Pressure vs. displacement for the sparse double dense model

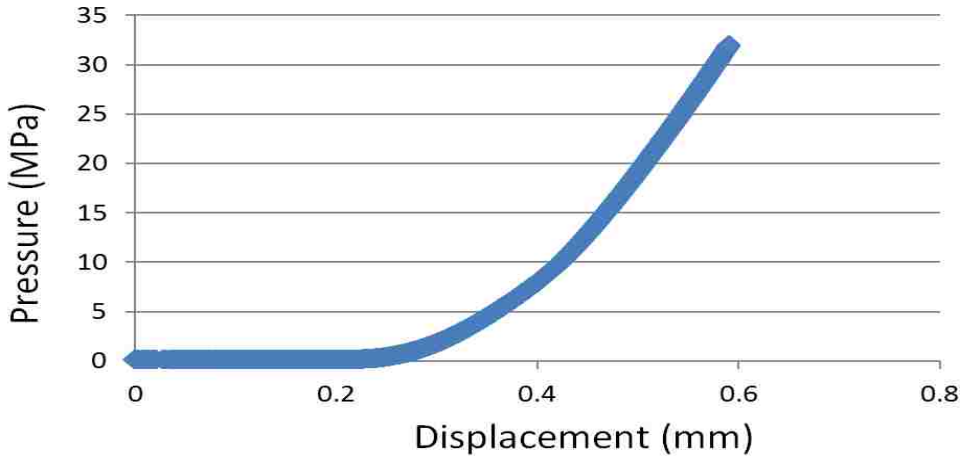

Figure 2.15 Pressure vs. displacement for the topology optimized model

The nonlinear graphs for the three different models are converted into linear relationships (Figure 2.16) in order to facilitate the comparison with the linear relationships used in the FEA results. The linear relationships derived from the FEA results are combined and compared on one chart, as shown in Figure 2.17. The chart includes a constant slope and a new "zero" for each curve to represent the ideal deformation starting point.

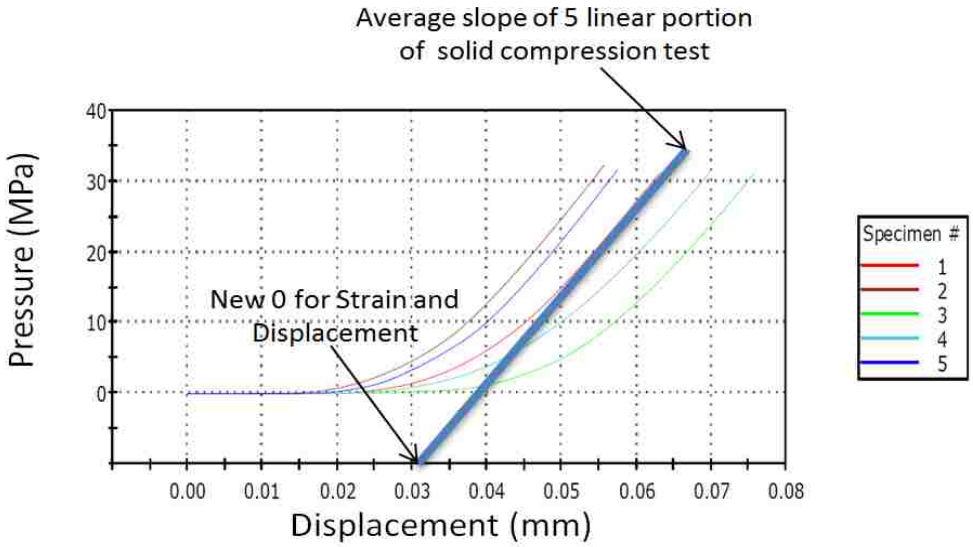

Figure 2.16 Illustration of average linearized result compared to nonlinear results

The average displacements at 20MPa, 22.5MPa, 25MPa, 27.5MPa, and 30MPa of pressure for each type of molding tool model are collected and a trend line is generated using the average value of displacement. Thus a fair comparison can be obtained for the different models. The equations for the solid, sparse double dense, and redesigned topology optimization models obtained are: 149.78x, 141.86x, and 120.78x, where x is the displacement in mm. Based on the slope equations, the sparse double dense model is 24% less stiff and the topology optimization model is 5.5% less stiff, in comparison to the solid model. The slope for each linear equation is then calculated with the detailed dataset, which is given in Appendix B.

The calculation of the slope shown in Figure 2.17 is done to obtain the stiffness using $k = P/\delta$, where P is the pressure and δ is the displacement. To calculate the percentage difference between the stiffness obtained from the FEA predictions and experiment data, the equation "percentage difference = $k_{FEA} / k_{solid} - 1$" is used.

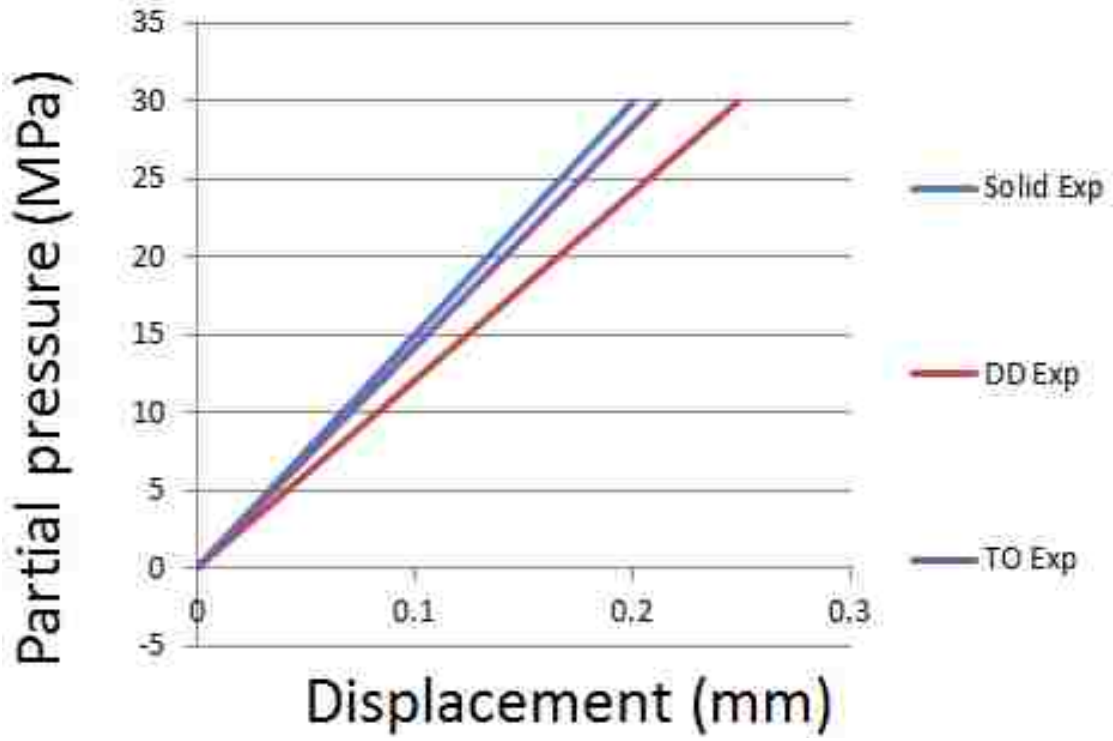

Figure 2.17 Linearized Pressure-displacement relationships

The percentage difference is the same at any load since a linear relationship is implemented. After five specimens of each model have been tested in the partial-pressure experiment, the comparison of FEA and experimental results is obtained as shown in Figure 2.18, which shows the difference of less than 10% between the FEA and experimental results for all three models. Therefore, the linear load-vs-displacement results from the FEA are considered accurate.

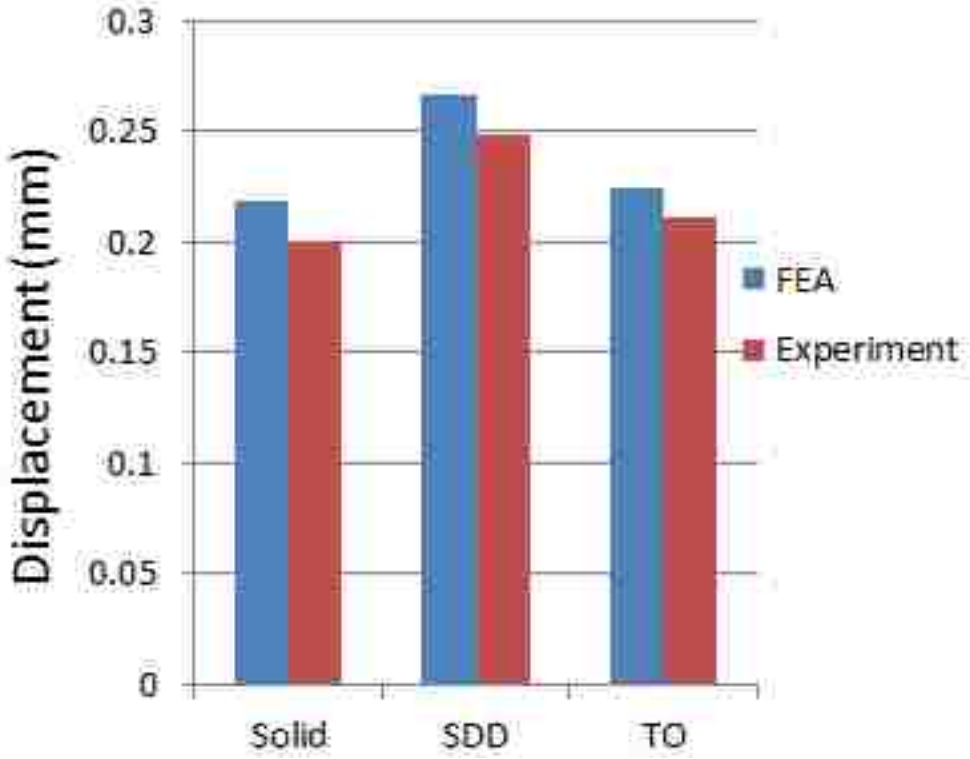

Figure 2.18 Displacement comparison between FEA and experiment with solid, sparse double dense, and topology optimized design

Since the difference between FEA predictions and experiment data is less than 10% on average, it is a good justification to trust the accuracy of the FEA solver. The differences can be due to fabrication tolerance, load sensor tolerance, and simulation

deviation. A coordinate measuring machine (CMM) is used to verify the geometry of the ULTEM 9085 testing tools.

A Brown & Shape RefleX 454 coordinate measuring machine shown in Figure 2.19 is used to measure the plastic deformation and verify the fabrication accuracy. The measurement is performed to verify the dimensions before and after the compression test.

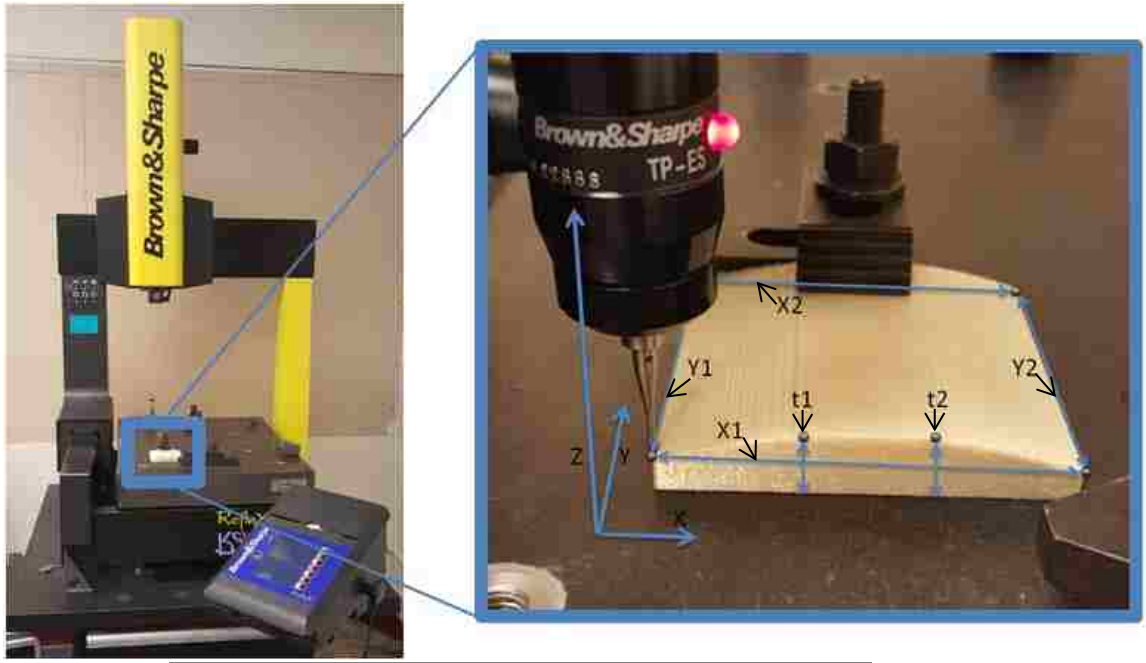

(a) (b)

Figure 2.19 (a) Brown & Sharpe RefleX 454 CMM; (b) illustration of dimensions measurements

To investigate the maximum plastic deformation, average dimension differences are measured before and after the compression experiment. The maximum plastic deformations occurred on the flat top surface for solid, sparse double dense, and topology optimized models are 0.5%, 0.22%, and 0.67% on average, respectively. Since the partial-pressure experiment shows a low plastic deformation at 30 MPa, the full-pressure model with 0.6895 MPa is expected to have a much lower plastic deformation.

Figure 2.20 shows that the fixture is adjusted to be as parallel to x-axis before the measurement begins. The horizontal coordinates are measured and a length is calculated as the difference between two points. For example, x1 = X_2-X_1, and y1 = Y_2-Y_1, where x1 and y1 are the horizontal and vertical lengths of the testing tool. X_1, Y_1, X_2 and Y_2 are the (x, y) coordinate readings from point 1, and point 2. The height of the flat top is calculated as the difference between the Z coordinates of the top surface and the stage. For example, t1 = $T_1 - T_{\text{stage reference}}$. After the dataset has been generated and calculated, the results are shown in Table 2.3 and Table 2.4. The detailed dataset obtained for calculating the averages is given in Appendix C.

Figure 2.20 Illustration of fixture calibration

Table 2.3 Partial-pressure model dimensions before compression test

	Before compression (mm)								
	Part	x1	y1	x2	y2	t1	t2	t3	t4
Solid	1	76.4921	76.4921	76.454	76.4286	9.17	9.17	9.17	9.17
	2	76.4794	76.4032	76.4921	76.4032	9.23	9.23	9.23	9.23
	3	76.581	76.4921	76.3905	76.4667	9.21	9.21	9.21	9.21
	4	76.4286	76.3778	76.2889	76.3397	9.14	9.14	9.14	9.14
	5	76.4667	76.3905	76.327	76.4032	9.25	9.25	9.25	9.25
Sparse double dense	6	76.5429	76.4413	76.454	76.4286	9.25	9.25	9.25	9.25
	7	76.454	76.4108	76.3524	76.4159	9.30	9.30	9.30	9.30
	8	76.4159	76.3397	76.4794	76.3905	9.30	9.30	9.30	9.30
	9	76.4794	76.3778	76.5302	76.3397	9.25	9.25	9.25	9.25
	10	76.454	76.4032	76.4286	76.3778	9.17	9.17	9.17	9.17
Topology optimization	11	76.3651	76.2	76.4286	76.073	9.21	9.21	9.21	9.21
	12	76.3524	76.2	76.4413	76.2	9.22	9.22	9.22	9.22
	13	76.3524	76.1746	76.3905	76.1873	9.21	9.21	9.21	9.21
	14	76.4032	76.2127	76.4032	76.2381	9.22	9.22	9.22	9.22
	15	76.3905	76.2	76.4413	76.2381	9.23	9.23	9.23	9.23

x1 & x2: Lengths of the part along the x-direction
y1 & y2: Lengths of the part along the y-direction
t1 & t2 : Tool heights along the z-direction

Table 2.4 Partial-pressure model dimensions after compression test

	After compression (mm)								
	Part	x1	y1	x2	y2	t1	t2	t3	t4
Solid	1	76.53	76.52	76.44	76.44	9.18	9.18	9.18	9.18
	2	76.54	76.39	76.58	76.45	9.26	9.26	9.26	9.26
	3	76.50	76.58	76.48	76.52	9.00	9.00	9.00	9.00
	4	76.39	76.38	76.29	76.35	9.11	9.11	9.11	9.11
	5	76.42	76.39	77.34	76.40	9.22	9.22	9.22	9.22
Sparse double dense	6	76.42	76.48	76.48	76.44	9.30	9.30	9.30	9.30
	7	76.44	76.42	76.42	76.35	9.25	9.25	9.25	9.25
	8	76.42	76.34	76.49	76.37	9.25	9.25	9.25	9.25
	9	76.52	76.35	76.52	76.35	9.21	9.21	9.21	9.21
	10	76.52	76.42	76.43	76.38	9.16	9.16	9.16	9.16
Topology optimization	11	76.29	76.52	76.20	76.31	9.17	9.17	9.17	9.17
	12	76.40	76.35	76.25	76.42	9.18	9.18	9.18	9.18
	13	76.25	76.34	76.35	76.25	9.16	9.16	9.16	9.16
	14	76.44	76.63	76.53	76.57	9.09	9.09	9.09	9.09
	15	76.29	76.39	76.21	76.37	9.18	9.18	9.18	9.18

x1 & x2: Lengths of the part along the x-direction
y1 & y2: Lengths of the part along the y-direction
t1 & t2 : Tool heights along the z-direction

3. FULL-PRESSURE MODEL OPTIMIZATION

3.1. TOPOLOGY OPTIMIZATION OF THE FULL-PRESSURE MODEL

The topology optimization of a full-pressure model is shown in Figure 3.1. The model has a pressure load of 0.6895 MPa on the top and side surfaces. A rigid flat plate is placed at the bottom. This study is intended to find out how the ULTEM 9085 molding tool behaves at room temperature (24^{o}C) influences the deformation and the von Mises stress.

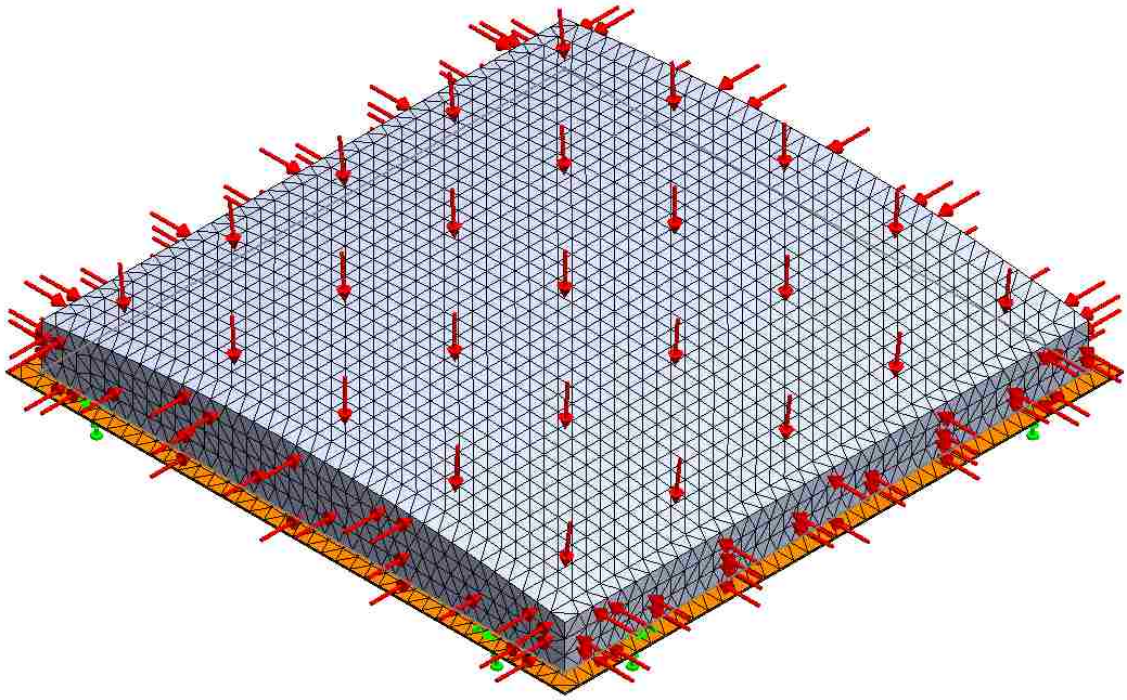

Figure 3.1 A pressure of 0.6895 MPa (100 psi) pressure evenly distributed on the top and side surfaces in topology optimization

The topology optimization study is completed with five different mesh sizes: low (10.16 mm), mid-low (5.08 mm), medium (2.54 mm), mid-high (1.27 mm), and high (1.15 mm). The results shown in Figure 3.2 show the tendency for the material to split up

into an increasing number of 0^o and 90^o thin walls, or stiffeners, when the mesh size is very small. Since the personal computer is not able to complete a study with extremely small meshes, a redesign is performed based on the convergence study of different number of stiffeners. After studying the rough topology optimization results, FEA studies are run to investigate the maximum deformation of the models generated by different mesh sizes.

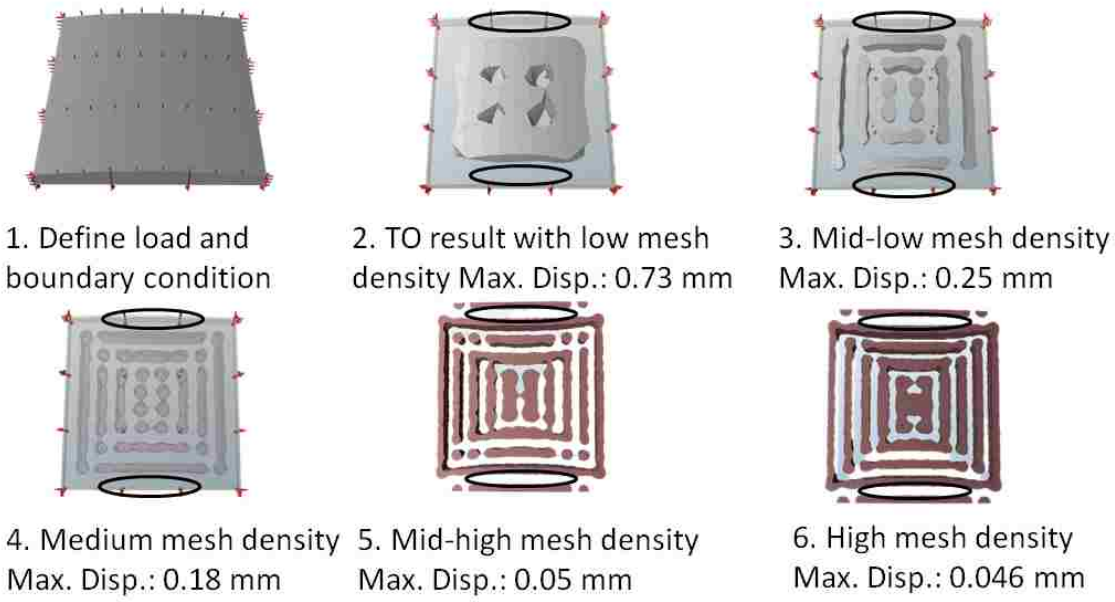

Figure 3.2 Illustration of topology optimization results with different mesh densities; black oval shows the location of maximum deformation

3.2. SMOOTHING AND GENERATION OF THE FULL-PRESSURE MODEL

The redesign is considered complete when the mesh is sufficiently small to describe an extrusion, and iteration pattern is implemented in the smooth redesign. From the topology optimization study, the higher mesh density results in a larger number of stiffeners. Therefore, a numerical investigation is conducted to study the compliance. After considering the manufacturability, a smoothed and simplified redesign is

implemented with equal width and equal airgap. Each model is adjusted to consume the same amount of material in the sparse double dense test tool. Models shown in Figure 3.3 are designed to have 5, 10, 15, and 20 stiffeners.

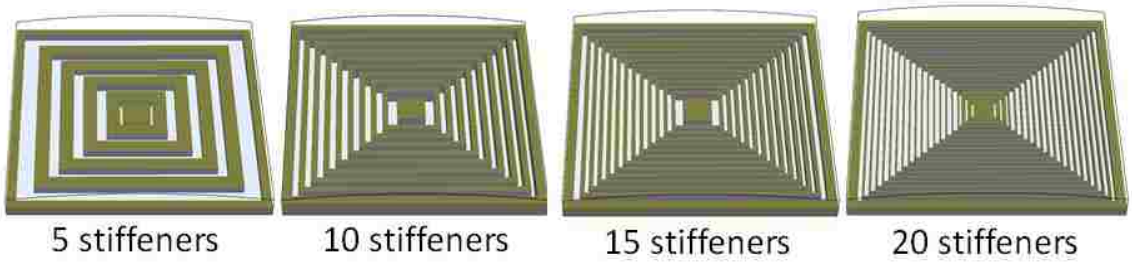

Figure 3.3 Illustration of redesigned topology optimization models with different numbers of stiffeners

3.3. FEA VALIDATION

After finishing FEA study for the first set of redesigned models, a chart is plotted to study the model's compliance. The mold with 10 stiffeners has the lowest results of maximum von Mises stress and displacement. To investigate a wide range of possibilities, models with 7, 8, 9, 11, 12 and 13 stiffeners are also studied. The maximum von Mises stress and maximum resultant displacement comparison is shown in Figure 3.4 and Figure 3.5. By comparing the redesigns based on topology optimization of 10 different stiffeners, it can be seen that the design with 10 stiffeners shown in Figure 3.6 is the optimal.

The performance of the best redesign from topology optimization is compared with the performances of solid and sparse double dense designs. The displacement in the z-direction is shown in Figure 3.7, where the dark blue color signifies the maximum displacement in the negative direction, or into the part, and the dark red color signifies the maximum displacement in the positive direction. The resultant displacements under full-pressure are compared for the three different designs in Figure 3.8, where the resultant displacement is the total displacement regardless of the direction. The maximum

resultant displacement is estimated to appear on the top curved edge on all designs since the resultant displacement is considering the combined displacement in x-, y-, and z-directions. The edges are deformed inward towards the center of the part due to the pressure on the sides. An interesting phenomenon is that the sparse double dense has dimples in the middle of the air gap, where there is no material directly supporting the shell; see Figure 3.9. A similar phenomenal happened to the topology optimized design in between the stiffeners.

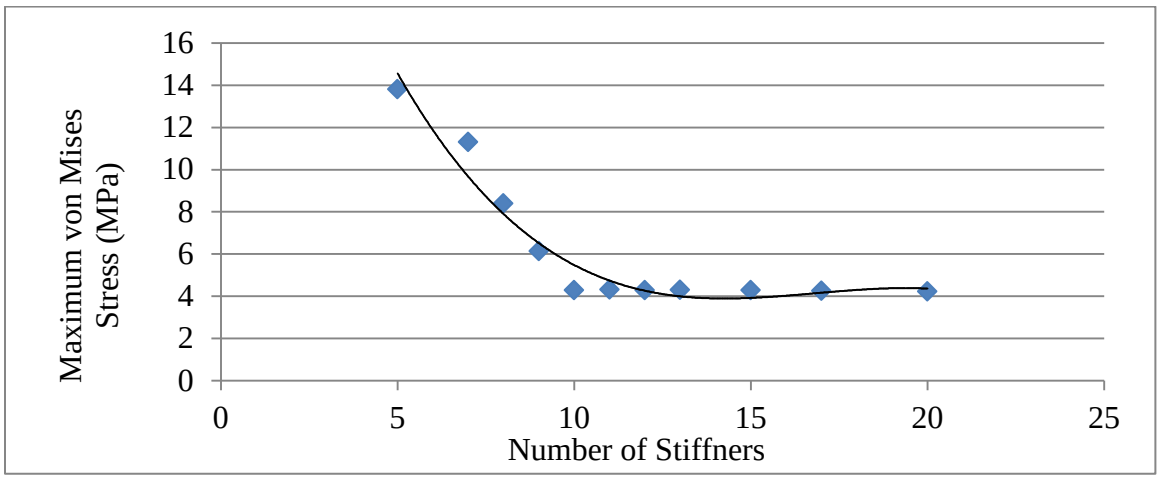

Figure 3.4 Maximum von Mises stresses with different number of stiffeners

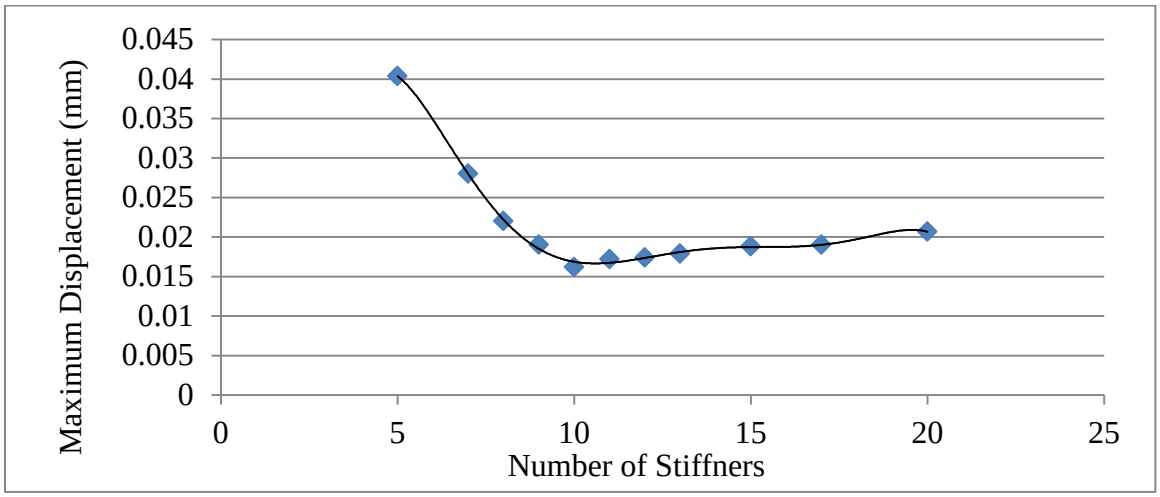

Figure 3.5 Maximum displacements with different number of stiffeners

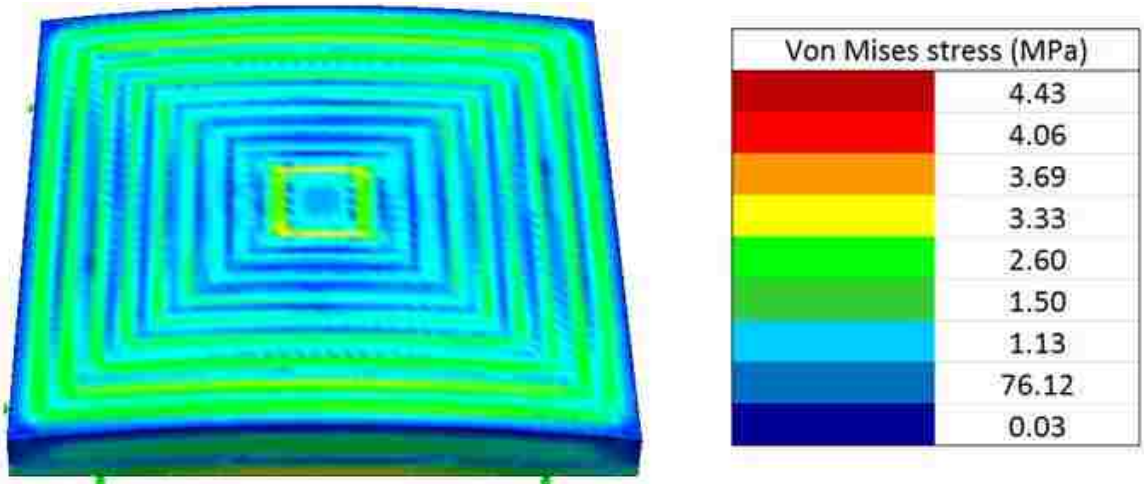

Figure 3.6 Illustration of von Mises stress with ten stiffeners

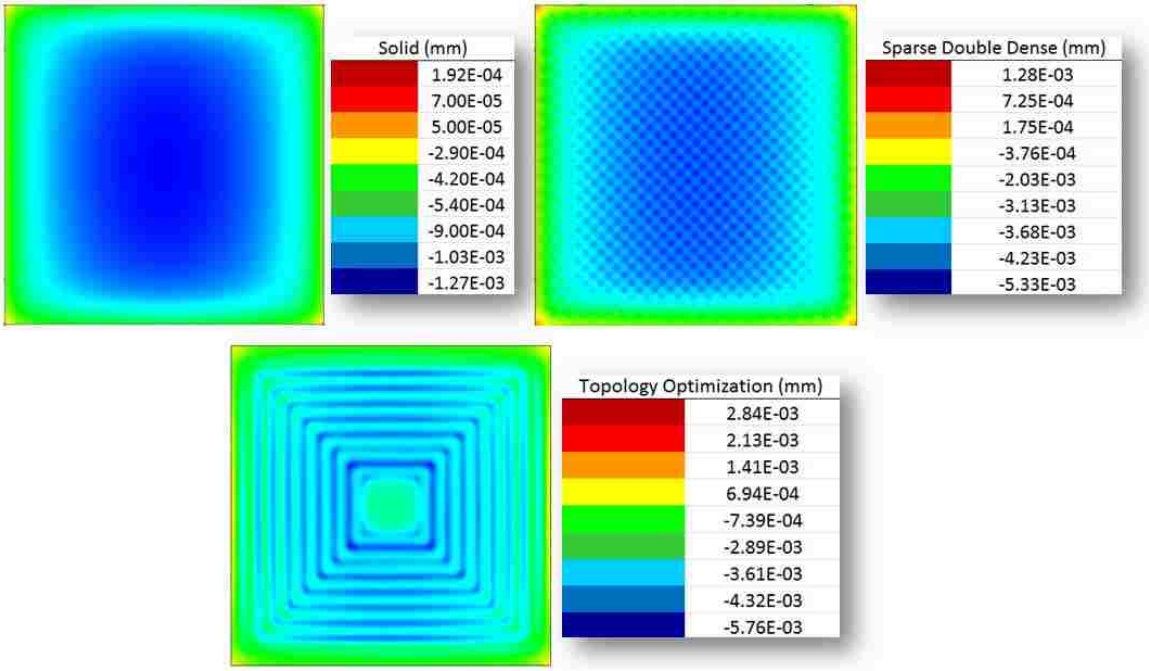

Figure 3.7 Illustrations of displacement in z-direction

Table 3.1 compares the fabrication and FEA simulation results of the full-pressuremodels with the three different structures. Although the sparse double dense

model has a lower maximum displacement than topology optimization, the topology optimization model is a safer structure under the full-pressure environment due to the lower maximum von Mises stress. Therefore, maximum displacement and maximum von Mises stress are tradeoff between these two designs. Since the redesigned topology optimization requires soft support material in between the stiffeners, the build time is longer than the other two designs. A FEA convergence analysis is studied to minimize the error determine the proper mesh size that is small enough to minimize the computational error and yet not too small to demand too much computation time and memory. The detailed convergence dataset obtained for the comparison is given in Appendix D.

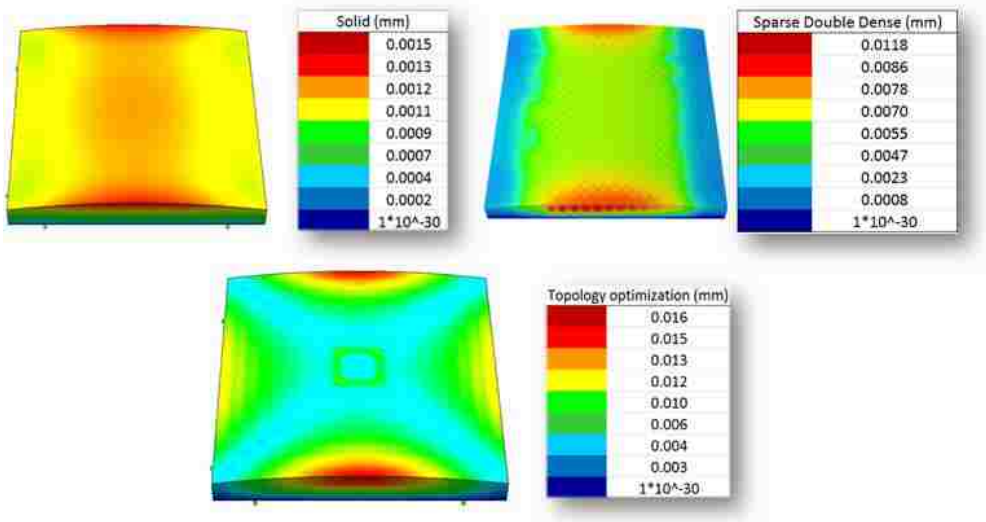

Figure 3.8 Illustrations of resultant displacement among the three different designs

Table 3.1 Fabrication and FEA simulation results of three full-pressure models

	Build Material (cm^3)	Support Material (cm^3)	Build Time (min)	Maximum Resultant Displacement (mm)	Maximum von Mises Stress (MPa)
Solid	44.41	1.64	48	0.00148	0.75
Sparse Double Dense	28.35	1.64	35	0.0118	4.51
Topology Optimization	28.35	9.99	111	0.0156	3.70

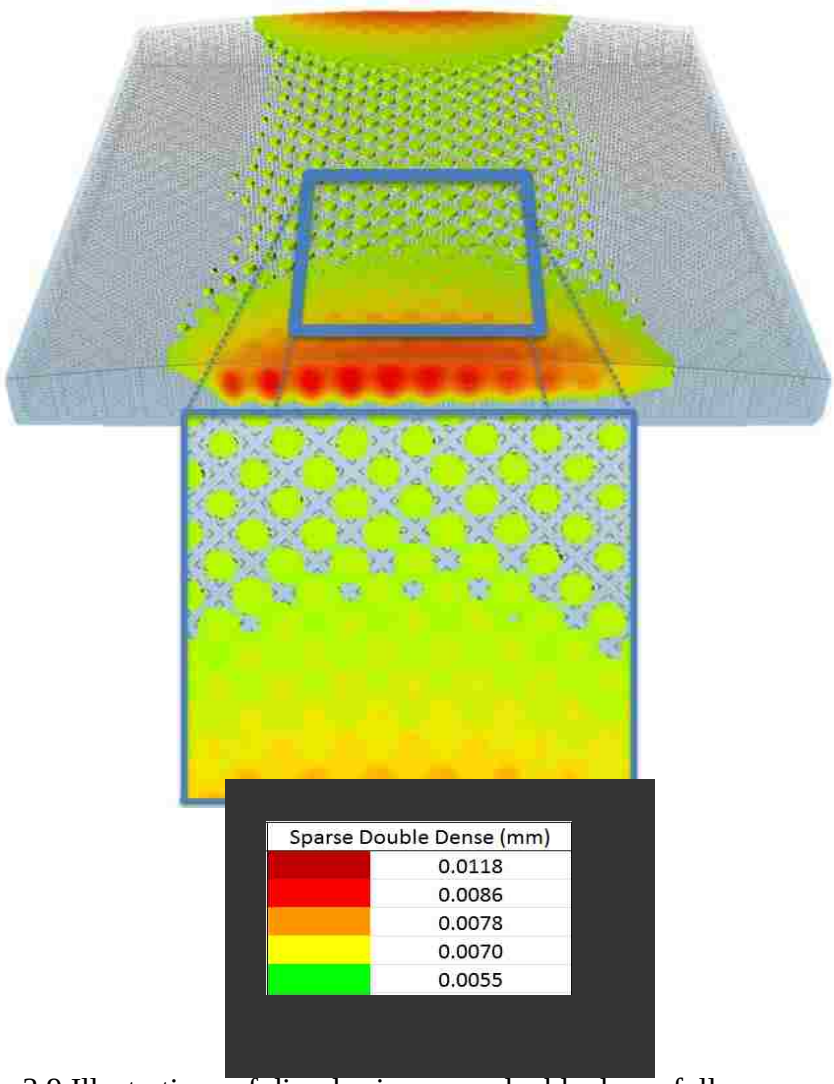

Figure 3.9 Illustrations of dimples in sparse double dense full-pressure FEA

4. OVERALL COMPARISON OF THE THREE DIFFERENT STRUCTURES

Solid, sparse double dense, and topology optimization for both partial-pressure and full pressure compression comparisons of six models in the FEA studies are shown in Figures 4.1 and 4.2. Depending on the application criteria, topology optimization may not be the ideal internal structure, even though it provides a performance that is close to a solid part in the partial-pressure compression experiment. In this experiment, both internal structures provide excellent stiffness and little deformation at room temperature.

The overall performance is compared using bar charts with five major performance criteria: 1) build material amount, 2) support material amount, 3) build time, 4) maximum von Mises stress, and 5) maximum resultant displacement. In different applications, the internal structure can be chosen based on the desired characteristics application requirements and the fabricating the physical models.

In the compression testing experiment, the solid internal structure offers the lowest displacement and highest safety factor. The solid internal structure consumes the most build material and is also the heaviest of the three designs. The sparse double dense internal structure has the shortest build time and does not use any support material in the final part, as in the case of the topology optimization model. The greatest disadvantage of the sparse double dense internal structure is the displacement, which is 17.9% more than the solid internal structure, and the safety factor is 75.3% lower than the solid internal structure. When build material amount and build time are the main concerns, the sparse double dense internal structure is the best for this application.

The topology optimization designs take the longest time to build out of the three structures in both partial and full-pressure models since support material is needed. Furthermore, it has a safety factor that is 18.9% lower than that of the solid internal structure, and the displacement is only 2.3% less than that of the solid internal structure. The topology optimization is the best internal structure in the partial-pressure model when build time is not a concern since the maximum displacement is close to the solid internal structure and consumes less material.

From the bar charts in Figure 4.1, the designer can select an internal structure for their design that satisfies their objectives and constraints. Although the topology optimization has a notable advantage over the sparse double dense internal structure in the partial-pressure models, the sparse double dense internal structure in the full-pressure FEA models outperformed the topology optimization method in terms of displacement.

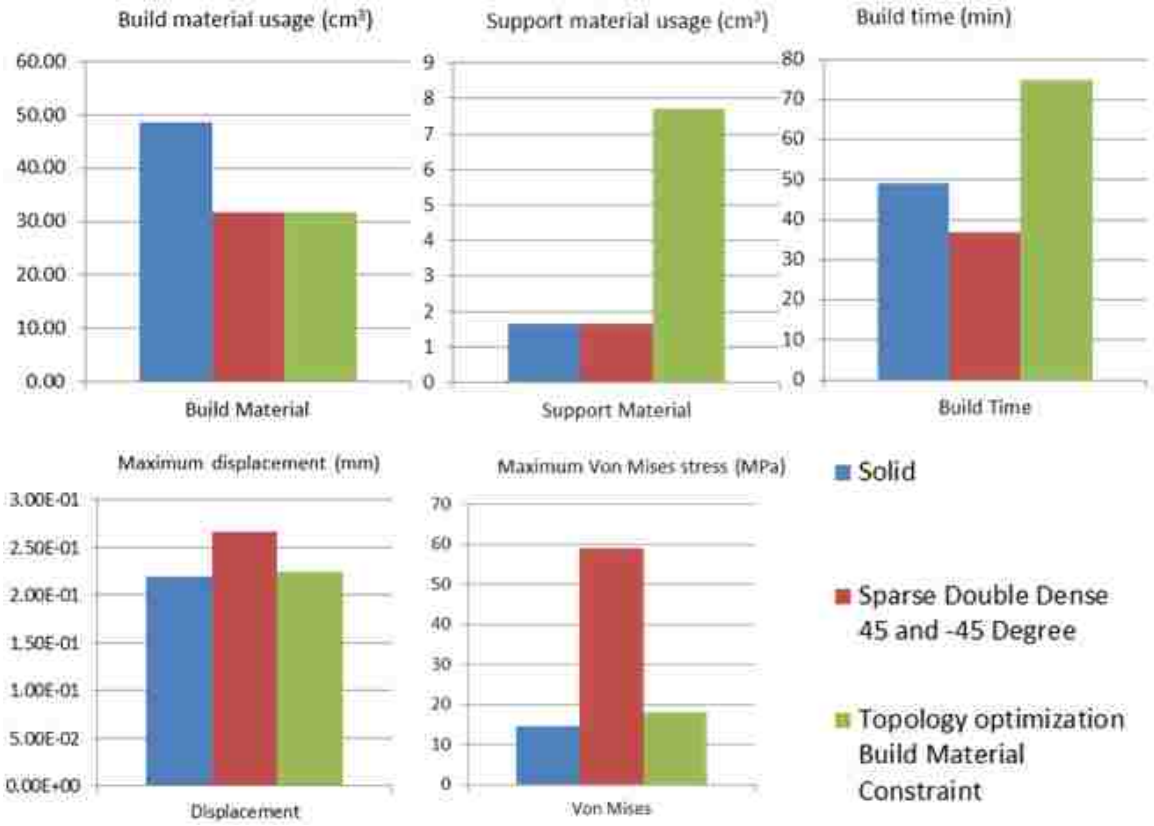

Figure 4.1 Overall FEA, fabrication performance comparison of the partial-pressure model

In the autoclave molding tool application comparison shown in Figure 4.2, although the solid model takes longer time than the sparse double dense model to build, it maintains its advantage with the lowest von Mises stress and displacement and has an evenly distributed displacement.

The sparse double dense internal structure has advantages regarding lower material usage and reduced build time. Compared to the solid internal structure, the von Mises stress is 98% higher and the maximum displacement is 87% higher. However, the safety factor with this internal structure is 1.41, and the displacement is 0.0186 mm, i.e., it is still safe and has a displacement that is considerably lower than 1% under 0.6895 MPa environment.

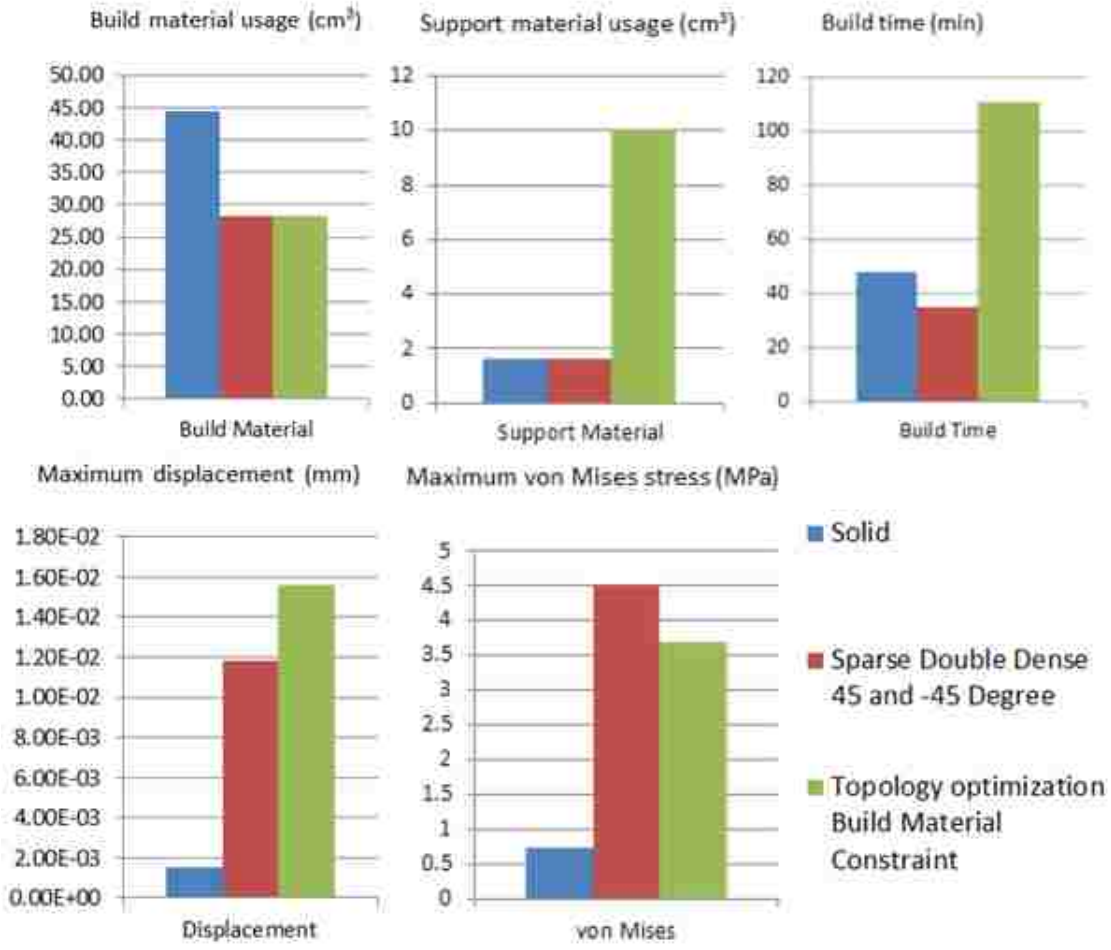

Figure 4.2 Overall FEA, fabrication performance comparison of the full-pressure model

The topology optimization model requires the longest time to manufacture in the autoclave molding tool application. Although it uses the same amount of build material as the sparse double dense internal structure, the build time is 68% longer than that of the sparse double dense internal structure because of the additional movement of the print head, additional support material, and additional starts and stops during extrusion. The maximum displacement and maximum von Mises stress are a tradeoff between the sparse double dense internal structure and topology optimization. Since the maximum von Mises stress is 21% lower with the topology optimization internal structure compared to the sparse double dense internal structure, this internal structure has a greater likelihood of withstanding an endurance test despite a slightly larger displacement.

Plastic deformation was negligible (0.46% at most) at 30 MPa. The pressure inside of an autoclave chamber only reaches 0.6895 MPa, which is far from that required to result in significant plastic deformation. Partial-pressure linear elastic deformation is accurately predicted by the FEA solver; thus, the full-pressure FEA study is also credible. The designs based on topology optimization showed a lower maximum von Mises stress in both models, however, this method does not take manufacturability into consideration. therefore fabrication time is not optimized. The detailed dataset obtained for the comparison is given in Appendix E.

5. CONCLUSION

This research investigates the performance of an autoclave molding tool fabricated by fused deposition modeling process using three different internal structures: solid, sparse double dense (SDD) structure, and topology optimization (TO) geometry. This research compares the solid model to the SDD and TO models, aimed to understand the use of these three different models to build the molding tool. The build material, support material, build time, maximum displacement, and maximum von Mises stress are compared between the three models, with an emphasis to contrast the pros and cons between the SDD and TO models.

The three different models are compared for an autoclave molding tool. For the molding tool studied, SDD takes the least amount of time to manufacture at 37 minutes, which is 27% less time than manufacture of the solid model and 62% less time than manufacture of the TO model. This is because TO creates an internal geometry that requires deposit6ing support material during the part fabrication process. The amount of part material used for both of the SDD and TO models is 32% less than that used for the solid model. The maximum von Mises stress existing in the SDD model due to the autoclave pressure is 4.51 MPa, which is 14% higher than the TO model. The maximum displacement of the SDD model is 0.012 mm, which is 14% less than the TO model. Minimizing the mold deformation (maximum displacement) and the dimpling (local indentation) of the mold due to the autoclave pressure exerting on the surface of the molding tool is critical to the quality of the finished composite parts. The maximum von Mises stress is critical if it may possibly exceed the yield stress with consideration of a safety factor. Compared to the TO molding tool, the SDD molding tool has better higher surface quality and takes less time to build (because they use the same amount of part material and the SDD tool uses significantly less support material).

APPENDIX A.

EXPERIMENT DATA OF COMPRESSION TEST WITH DIFFERENT BUILDING PARAMETERS

Table A.1 Parameters used in factorial compression experiment [2]

Part #	Compression Test				Flexure Test			
	Sparse fill air gap (in)	Wall thickness (in)	Cap layer thickness (in)	Porosity (Sdd) (%)	Sparse fill air gap (in)	Wall thickness (in)	Cap layer thickness (in)	Porosity (Sdd) (%)
P1	0.1	0.04	0.04	45.34	0.1	0.04	0.04	24.00
P2	0.1	0.04	0.05	44.22	0.1	0.04	0.05	20.00
P3	0.1	0.04	0.06	43.31	0.1	0.04	0.06	16.80
P4	0.1	0.06	0.04	42.34	0.1	0.06	0.04	22.40
P5	0.1	0.06	0.05	41.28	0.1	0.06	0.05	18.40
P6	0.1	0.06	0.06	40.38	0.1	0.06	0.06	15.20
P7	0.1	0.08	0.04	39.38	0.1	0.08	0.04	20.80
P8	0.1	0.08	0.05	38.52	0.1	0.08	0.05	17.60
P9	0.1	0.08	0.06	37.59	0.1	0.08	0.06	13.60
P10	0.15	0.04	0.04	55.35	0.15	0.04	0.04	30.40
P11	0.15	0.04	0.05	54.14	0.15	0.04	0.05	25.60
P12	0.15	0.04	0.06	52.91	0.15	0.04	0.06	21.60
P13	0.15	0.06	0.04	52.57	0.15	0.06	0.04	28.00
P14	0.15	0.06	0.05	51.38	0.15	0.06	0.05	24.00
P15	0.15	0.06	0.06	50.25	0.15	0.06	0.06	20.00
P16	0.15	0.08	0.04	49.40	0.15	0.08	0.04	26.40
P17	0.15	0.08	0.05	48.28	0.15	0.08	0.05	22.40
P18	0.15	0.08	0.06	47.21	0.15	0.08	0.06	18.40
P19	0.2	0.04	0.04	59.48	0.2	0.04	0.04	33.60
P20	0.2	0.04	0.05	58.15	0.2	0.04	0.05	28.80
P21	0.2	0.04	0.06	56.78	0.2	0.04	0.06	24.00
P22	0.2	0.06	0.04	56.16	0.2	0.06	0.04	31.20
P23	0.2	0.06	0.05	54.99	0.2	0.06	0.05	27.20
P24	0.2	0.06	0.06	53.82	0.2	0.06	0.06	22.40
P25	0.2	0.08	0.04	53.94	0.2	0.08	0.04	29.60
P26	0.2	0.08	0.05	52.81	0.2	0.08	0.05	24.80
P27	0.2	0.08	0.06	51.57	0.2	0.08	0.06	20.80

Table A.2 Compression test experiment results of 27 factorial parameter built parts [2]

Part #	Weight (Sdd) (g)	Porosity (Sdd) (%)	Yield strength (Sdd)	Compressive modulus (Sdd) (MPa)	Strength /weight ratio (Sdd)	Modulus/ weight ratio (Sdd)
P1	18.35	45.34	30.18	736.33	1.64	40.13
P2	18.72	44.22	30.66	737.00	1.64	39.37
P3	19.03	43.31	30.74	740.33	1.62	38.90
P4	19.35	42.34	32.65	763.33	1.69	39.45
P5	19.71	41.28	32.59	770.00	1.65	39.07
P6	20.01	40.38	32.72	774.67	1.64	38.71
P7	20.35	39.38	34.17	792.67	1.68	38.95
P8	20.63	38.52	34.29	800.67	1.66	38.81
P9	20.95	37.59	34.57	803.67	1.65	38.36
P10	14.99	55.35	21.15	575.67	1.41	38.40
P11	15.39	54.14	21.40	570.67	1.39	37.08
P12	15.80	52.91	21.45	577.00	1.36	36.52
P13	15.92	52.57	22.60	607.00	1.42	38.13
P14	16.32	51.38	22.94	609.00	1.41	37.32
P15	16.70	50.25	23.20	609.00	1.39	36.47
P16	16.98	49.40	25.30	643.67	1.49	37.91
P17	17.36	48.28	25.50	648.33	1.47	37.35
P18	17.72	47.21	25.44	648.67	1.44	36.61
P19	13.60	59.48	18.55	531.67	1.36	39.09
P20	14.04	58.15	18.88	537.00	1.34	38.25
P21	14.51	56.78	19.24	543.00	1.33	37.42
P22	14.71	56.16	20.56	564.00	1.40	38.34
P23	15.11	54.99	20.62	579.00	1.36	38.32
P24	15.50	53.82	20.73	586.33	1.34	37.83
P25	15.46	53.94	23.60	590.67	1.53	38.21
P26	15.84	52.81	23.54	608.00	1.49	38.38
P27	16.25	51.57	23.92	612.00	1.47	37.66

APPENDIX B.
VALIDATION TESTING TOOLS MAXIMUM DISPLACEMENTS

Table B.1 Average displacements of specimens with new “zero” at given pressure

	Displacement (mm)					
Solid (Mpa)	#1	#2	#3	#4	#5	Avg
20	0.499	0.426	0.614	0.555	0.449	0.508
22.5	0.518	0.444	0.632	0.574	0.466	0.527
25	0.536	0.462	0.651	0.594	0.483	0.545
27.5	0.554	0.480	0.670	0.613	0.501	0.564
30	0.572	0.497	0.689	0.633	0.518	0.582
Sparse double dense (Mpa)	#1	#2	#3	#4	#5	Avg
20	0.500	0.455	0.466	0.483	0.556	0.492
22.5	0.520	0.476	0.487	0.503	0.578	0.513
25	0.541	0.496	0.507	0.523	0.599	0.533
27.5	0.562	0.517	0.528	0.544	0.620	0.554
30	0.583	0.538	0.548	0.564	0.642	0.575
Topology optimization (Mpa)	#1	#2	#3	#4	#5	Avg
20	0.513	0.497	0.508	0.592	0.501	0.522
22.5	0.531	0.515	0.526	0.610	0.519	0.540
25	0.548	0.532	0.544	0.628	0.536	0.558
27.5	0.566	0.550	0.561	0.646	0.554	0.575
30	0.583	0.567	0.579	0.663	0.571	0.593

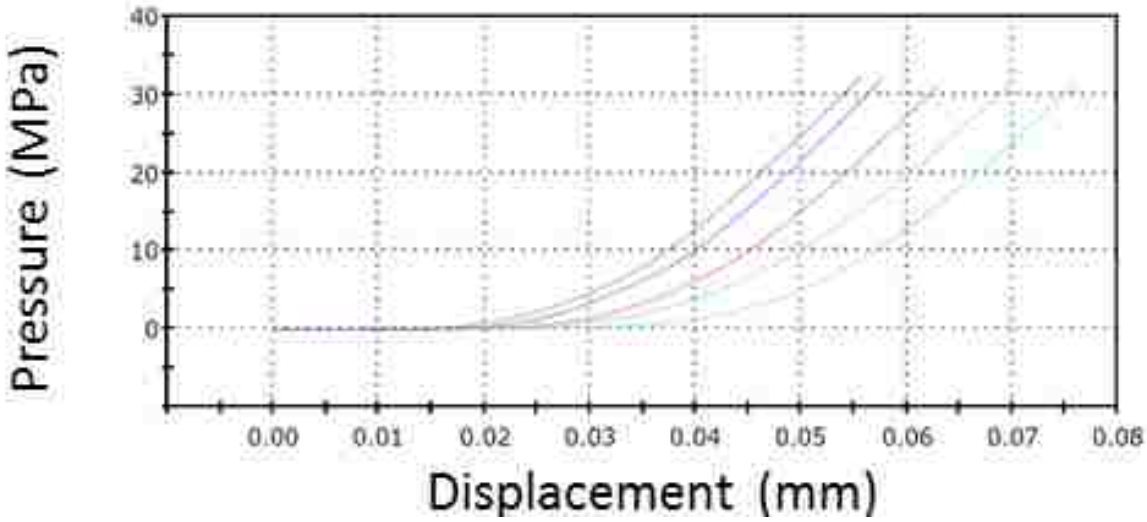

Figure B.1 Average solid pressure vs. displacement

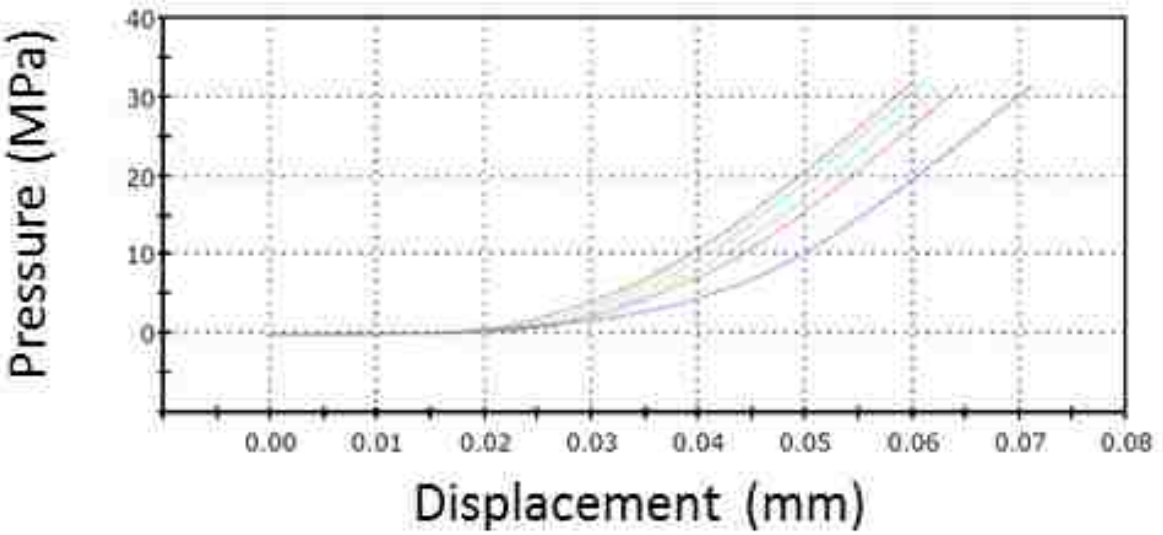

Figure B.2 Average sparse double dense pressure vs. displacement

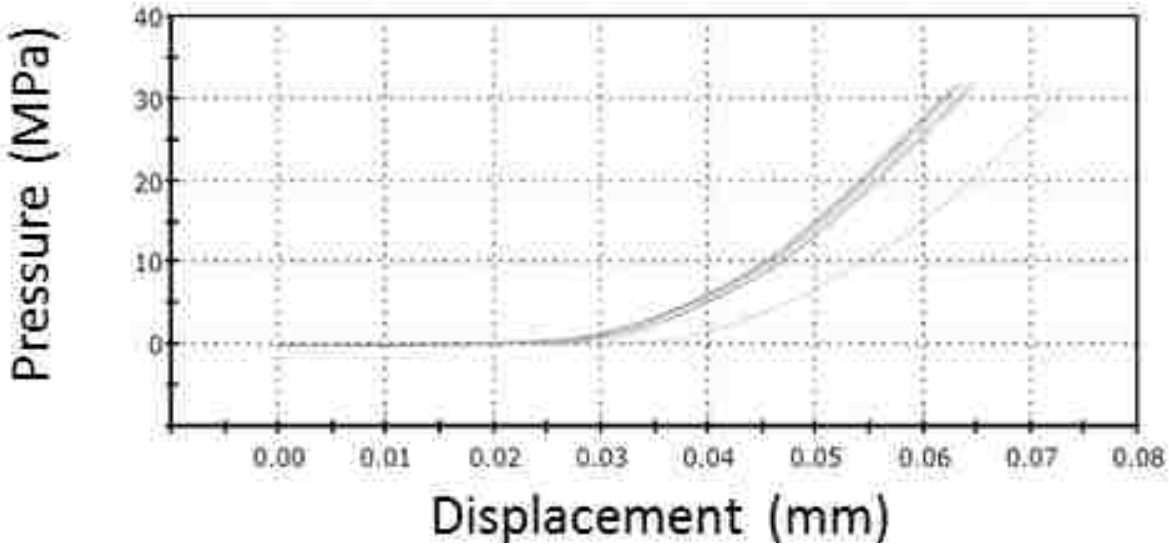

Figure B.3 Average redesign topology optimization pressure vs. displacement

APPENDIX C.
COORDINATE MEASUREMENT MACHINE DATA

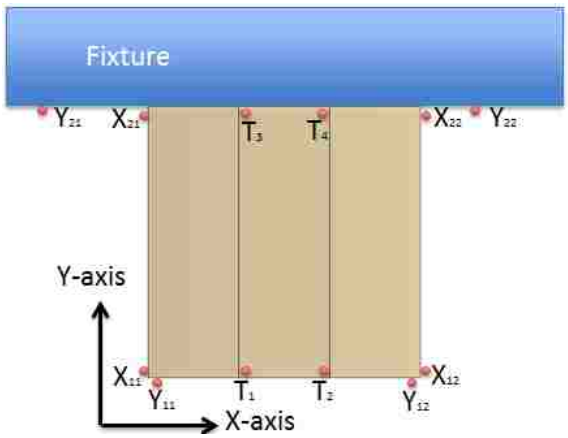

Figure C.1 Illustration of locations of coordinate measurements

Table C.1 Coordinate measurements before and after compression test

Before compression experiment (in)													
Part	X11	X12	X21	X22	Y11	Y12	Y21	Y22	T1	T2	T3	T4	Tstage
1	2.277	5.289	2.278	5.288	2.138	2.132	5.149	5.141	14.872	14.872	14.872	14.872	14.511
2	2.027	5.038	2.029	5.040	2.144	2.140	5.152	5.148	14.875	14.875	14.875	14.875	14.511
3	2.216	5.231	2.214	5.222	2.132	2.133	5.143	5.143	14.873	14.873	14.873	14.873	14.511
4	2.433	5.442	2.431	5.435	2.139	2.147	5.146	5.152	14.871	14.871	14.871	14.871	14.511
5	2.168	5.179	2.167	5.172	2.137	2.138	5.144	5.146	14.874	14.874	14.874	14.874	14.510
6	2.477	5.491	2.478	5.488	2.142	2.137	5.151	5.146	14.876	14.876	14.876	14.876	14.510
7	2.122	5.132	2.122	5.128	2.137	2.132	5.145	5.140	14.874	14.874	14.874	14.874	14.510
8	2.188	5.197	2.189	5.200	2.149	2.135	5.154	5.142	14.873	14.873	14.873	14.873	14.509
9	2.267	5.278	2.268	5.281	2.144	2.147	5.151	5.152	14.871	14.871	14.871	14.871	14.509
10	2.402	5.412	2.402	5.411	2.132	2.135	5.140	5.142	14.869	14.869	14.869	14.869	14.509
11	2.464	5.471	2.464	5.473	2.149	2.146	5.149	5.141	14.869	14.869	14.869	14.869	14.508
12	2.178	5.184	2.178	5.187	2.148	2.146	5.148	5.146	14.870	14.870	14.870	14.870	14.508
13	2.261	5.267	2.259	5.267	2.142	2.155	5.141	5.154	14.869	14.869	14.869	14.869	14.508
14	2.281	5.289	2.281	5.289	2.148	2.139	5.148	5.140	14.867	14.867	14.867	14.867	14.509
15	2.079	5.087	2.077	5.087	2.143	2.153	5.143	5.154	14.871	14.871	14.871	14.871	14.509
After compression experiment (in)													
Part	X11	X12	X21	X22	Y11	Y12	Y21	Y22	T1	T2	T3	T4	Tstage
1	2.072	5.085	2.074	5.083	2.135	2.135	5.146	5.144	14.872	14.872	14.872	14.872	14.511
2	2.037	5.051	2.038	5.053	2.134	2.141	5.142	5.151	14.875	14.875	14.875	14.875	14.511
3	2.114	5.126	2.113	5.124	2.140	2.131	5.145	5.143	14.865	14.865	14.865	14.865	14.511
4	2.423	5.431	2.423	5.426	2.145	2.148	5.151	5.154	14.869	14.869	14.869	14.869	14.511
5	2.138	5.147	2.137	5.182	2.144	2.140	5.152	5.148	14.874	14.874	14.874	14.874	14.511
6	2.350	5.359	2.350	5.361	2.141	2.131	5.153	5.140	14.875	14.875	14.875	14.875	14.511
7	2.230	5.240	2.230	5.239	2.139	2.136	5.145	5.142	14.877	14.877	14.877	14.877	14.511
8	2.121	5.130	2.122	5.133	2.147	2.135	5.152	5.141	14.877	14.877	14.877	14.877	14.511
9	2.279	5.292	2.279	5.292	2.135	2.139	5.152	5.145	14.875	14.875	14.875	14.875	14.511
10	2.470	5.483	2.471	5.480	2.137	2.141	5.144	5.148	14.872	14.872	14.872	14.872	14.511
11	2.152	5.156	2.152	5.152	5.149	2.143	5.149	5.147	14.873	14.873	14.873	14.873	14.511
12	2.379	5.387	2.377	5.379	5.141	2.135	5.141	5.143	14.874	14.874	14.874	14.874	14.511
13	2.068	5.070	2.068	5.074	5.154	2.148	5.154	5.150	14.874	14.874	14.874	14.874	14.511
14	2.164	5.174	2.165	5.178	5.149	2.135	5.149	5.149	14.875	14.875	14.875	14.875	14.512
15	2.230	5.234	2.230	5.231	5.153	2.144	5.153	5.150	14.875	14.875	14.875	14.875	14.512

APPENDIX D.
FINITE ELEMENT ANALYSIS CONVERGENCE STUDY

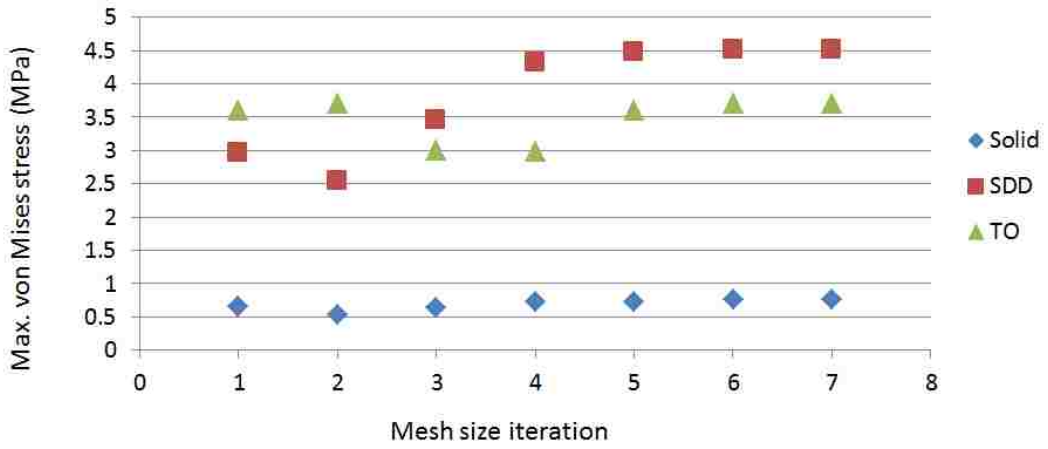

Figure D.1 Illustration of FEA maximum von Mises stress convergence

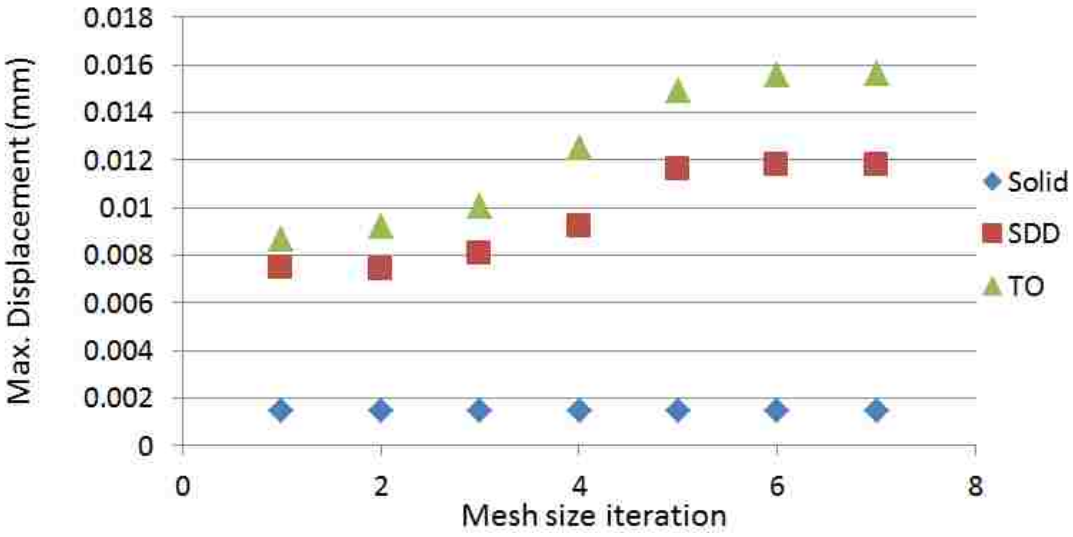

Figure D.2 Illustration of FEA maximum displacement convergence

Table D.1 Full-pressure model iteration mesh sizes

Mesh size Iteration	1	2	3	4	5	6	7
Solid (mm)	0.2	0.1	0.05	0.044	0.038	0.031	0.025
SDD (mm)	0.2	0.15	0.1	0.05	0.04	0.03	0.025
TO (mm)	0.4	0.3	0.25	0.2	0.15	0.1	0.078

APPENDIX E.
BAR CHART DATA

Table E.1 Partial-pressure bar chart comparison data

	Amount of Material (cm^3)		Percent of Build Material Reduced	Build Time (min)	Finite Element Analysis	
	Build	Support			Maximum Displacement @ 30 MPa (mm)	Maximum von Mises Stress (MPa)
Solid	48.51	1.64	0%	49	2.19E-01	14.651
Sparse Double Dense	31.79	1.64	34.45%	37	2.67E-01	59.136
Topology Optimization	31.79	7.7	34.45%	75	2.24E-01	18.064

Table E.2 Full-pressure bar chart comparison data

	Amount of Material (cm^3)		Percent of Build Material Reduced	Build Time (min)	Finite Element Analysis	
	Build	Support			Maximum Displacement @ 30 MPa (mm)	Maximum von Mises Stress (MPa)
Solid	44.41	1.64	0%	48	1.48E-03	0.750
Sparse Double Dense	28.35	1.64	36.16%	35	**9.39E-03**	**5.161**
Topology Optimization	28.35	9.99	36.16%	111	**1.60E-02**	**4.429**

BIBLIOGRAPHY

1. Chua, C. K., Leon, K. F. and C., Lim, S, "Rapid prototyping: Principles and Applications," Rapid Prototyping 2nd edition, World Scientific, Singapore, Vol. 1, pp 124-129, 2003
2. Iyibilgin, O., Leu M. C., Taylor G., Li, H., and Chandrashekhara, K., "Investigation of Sparse-Build Rapid Tooling by Fused Deposition Modeling," In: Proceedings of the Solid Freeform Fabrication Symposium, Austin, TX, pp 542-556, 2014
3. http://usglobalimages.stratasys.com/Main/Files/Best%20Practices_BP/BP_FDM_VariableDensity.pdf?v=635817995040925513, Last accessed on 12/20/2015
4. Browne, P. A., "Topology Optimization of Linear Elastic Structures," University of Bath, PhD Thesis, 2013
5. Bendsoe, M. P., Sigmund, O., "Topology Optimization: Theory, Methods and Applications," Springer Science & Business Media, Berlin, Heidelberg, 2002
6. Li, H., Taylor G., Bheemreddy V., Iyibilgin O., Leu M. C., and Chandrashekhara K., "Modeling and characterization of fused deposition modeling tooling for vacuum assisted resin transfer molding process," Additive Manufacturing, Vol. 7, pp 64-72, 2015
7. http://usglobalimages.stratasys.com/Main/Files/White%20Papers/WP_FDM_Fortus360mc400mcAccuracyStudy.pdf?v=635787005291964002, Last accessed on 12/20/2015
8. http://www.instron.us/en-us/our-company/library/glossary/c/compression-test, Last accessed on 12/20/2015
9. http://help.solidworks.com/2014/english/solidworks/cworks/c_analysis_solvers.htm, Last accessed on 12/20/2015
10. http://www.stratasys.com/materials/fdm/~/media/83DA2BBEE7DE4A669CFEF6B1FCA118AA.ashx, Last accessed on 12/20/2015
11. Leu, M. C., and Chandrashekhara K., "Sparse-build rapid tooling by fused deposition modeling for composite manufacturing and hydroforming," America Makes, 2014
12. http://www.hexcel.com/Resources/DataSheets/Brochure-Data-Sheets/Honeycomb_Sandwich_Design_Technology.pdf, Last accessed on 1/20/2016

VITA

The Author of this thesis, Shixuan Meng, received his Bachelor's degree in Mechanical Engineering from Missouri University of Science and Technology, Rolla, Missouri, United States, in May 2013. After spending seven months at Nortek Global HVAC, and published a U.S patent He joined the Master of Science program in Mechanical Engineering at Missouri University of Science and Technology in January 2014. The author received his Master of Science degree in Mechanical Engineering from Missouri University of Science and Technology in May 2016.